Summer 2012

Adsorption of citric acid on cerium oxide nanoparticles (nanoceria) : effects of pH, surface charge and aggregation

Induni Wathsala Siriwardane
University of Iowa

ADSORPTION OF CITRIC ACID ON CERIUM OXIDE NANOPARTICLES (NANOCERIA): EFFECTS OF pH, SURFACE CHARGE AND AGGREGATION

by

Induni Wathsala Siriwardane

A thesis submitted in partial fulfillment
of the requirements for the
Master of Science degree in Chemistry
in the Graduate College of
The University of Iowa

July 2012

Thesis Supervisor: Professor Vicki H. Grassian

Graduate College
The University of Iowa
Iowa City, Iowa

CERTIFICATE OF APPROVAL

MASTER'S THESIS

This is to certify that the Master's thesis of

Induni Wathsala Siriwardane

has been approved by the Examining Committee
for the thesis requirement for the
Master of Science degree in Chemistry
at the July 2012 graduation.

Thesis Committee: _____
Vicki H. Grassian, Thesis Supervisor

_____
Sarah C. Larsen

_____
Amanda J. Haes

To my ever loving parents
for molding their ‘little girl’ into a ‘strong woman’,
who can smile at
every challenge on her way

ACKNOWLEDGMENTS

Foremost I would like to express my gratitude to my supervisor, Professor Vicki H. Grassian for the guidance and support given to me to make this project successful. Also I would like to thank to my committee members, Professor Sarah Larsen and Professor Amanda Haes for their valuable support.

I am also thankful to the US Environmental Protection Agency for funding this research. Further, I would like to thank Dr. Jonas Baltrusaitis for the support given in XPS measurements. And also my appreciation goes to the staff members of the Chemistry Stores and the Electrical Shop of the Department of the Chemistry of the University of Iowa for their kind assistance provided.

A special word of thanks should be given to all present and former Grassian group members for their kind support given to me throughout this period of one and half years. Especially I would like to thank Imali Mudunkotuwa, Thilini Rupasinghe and Dr. Larissa Stebanovna for their immense support.

Furthermore I would like to thank all my colleagues here at Iowa for their helping hands for me. A special word of thank should be gone to my Sri Lankan friends here at UIowa for being with me and supporting with everything throughout this period.

Last but not least I would like to thank my loving husband, parents and my family for encouraging me at every moment. The emotional strength you all gave me was the giant shade behind all my achievements.

ABSTRACT

Among a large number of engineered nanomaterials, CeO_2 nanoparticles (nanoceria) are of particular interest due to their unique oxidative, optical and electrical properties. With the increasing use of this important rare-earth metal oxide nanoparticle, there is the potential for it to be released in to the environment. Surface adsorbed ligands affect the surface chemistry of nanomaterials and thereby ultimately determine their fate and transformation in the natural environment. Citric acid is a naturally abundant organic acid, which can play an important role in determining the environmental fate of nanomaterials. This study focuses on citric acid adsorption onto nanoceria for three different particle diameters of 4, 9 and 39 nm. Both the details of surface adsorption of citric acid at different pH and its impact on nanoparticle behavior are explored. Speciation of adsorbed citric acid as a function of pH is probed using ATR-FTIR measurements, whereas HPLC and X-ray photoelectron spectroscopy are used to quantify the adsorption coverage. These results show that the surface speciation of citric acid differs from that of bulk solution at all pHs studied and the coordination to the surface as well as surface coverage is a function of particle size. Nanoparticle-nanoparticle interactions and suspension stabilities are further probed through sedimentation and zeta potential measurements to better understand the behavior of ceria nanoparticles with and without the presence of citric acid.

TABLE OF CONTENTS

LIST OF TABLES

LIST OF FIGURES

CHAPTER 1

INTRODUCTION

1.1 Nanoscience and Nanotechnology

Nanoscience is not merely a branch of modern science, but it is becoming the basis for many of the technologies used today. Although nanotechnology has the potential to revolutionize most of the industries in the world, the use of nano-dimension particles and materials is not new.[1, 2] For example, the use of Au nanoparticles (NPs) as an inorganic dye in Chinese ceramic industry has a history of more than a thousand years; and colloidal gold has been used in some medical applications.[1] Since Richard Feyman's speech in 1959, followed by Norio Taniguchi's introduction of the word "nanotechnology" in 1974, the definition of nanotechnology has been a topic of many discussions for some time.[1] In the United States, it is defined as being "concerned with materials and systems whose structures and components exhibit novel and significantly improved physical, chemical and biological properties, phenomena and processes due to their nanoscale size".[1] However, despite its long history, the rapid development of tools to manipulate these nanoscale materials is what has made it a hot area of research recently. Consequently, nanomaterials are being found in a variety of areas such as electronic, biomedical, pharmaceutical, cosmetic, energy, environmental, catalytic and material applications.[2]

In a technology, which centers around the unique properties of particulate matter derived from their small size, understanding and control of particle size and morphology

becomes essentially important. Nanoparticles, the matter at dimensions of 1-100 nm, exist and now are being synthesized in numerous shapes such as spherical, tubular, rod-like or irregular and exist in fused, aggregated or agglomerated forms. One main categorization of NPs based on their origin is into natural and anthropogenic (engineered) nanoparticles. Engineered nanoparticles (ENPs) can be again broadly categorized into carbon-based ENPs and mineral ENPs. In general, ENPs include fullerenes, metals, oxides, quantum dots, organic polymers and complex compounds such as, nanofluids, alloys and composites. It is expected a production of 58000 tons of ENPs in 2011-2020.[2]

Among the wide variety of ENPs, metal and metal oxide nanoparticles are being increasingly used in many fields such as catalysis, environmental remediation,

Table 1.1. Examples of metal-based nanomaterial applications

Metal-based nanomaterial	Applications
Ag	Antibacterial and disinfecting agent (textiles, healthcare, refrigerators, air conditioners, washing machines), anti-corrosive coating (paints and coatings), microelectronic industry (wiring, encapsulation and connectors), catalysis.
Al, Al_2O_3	Catalyst supports, antibacterial and disinfecting agent (textile, plastics, coatings), transparent conductive and optical coating (optical lenses, window and flooring), wear-resistant additive, heat transfer fluid, cosmetic filler, water-proof material.

Table 1.1. Continued

CeO_2	Catalysis and catalyst supports, solid oxide fuel cells (electrode materials), sintering additives, heat resistant alloy coatings, UV absorbent, superconducting materials (buffer layer).
Cu, CuO	Antibacterial and disinfecting agent, (textiles plastics and coatings), microelectronic industry (wiring and connections), catalysis (rocket propellant combustion), gas sensors, thermoelectronics, superconductors.
Fe, Fe_2O_3, Fe_3O_4	Environment remediation (removal of actinides from waste water), magnetic data storage, biomedical applications (MRI contrast agents, magnetic separations, targeted drug delivery), semiconductor, microwave devices.
TiO_2	Photocatalysis, antibacterial and disinfecting agent (paint and coatings, ceramics, glass), cosmetics, UV resistors (sunscreens), air purification, semiconductors, astronautics, solar cells.
ZnO	Electronic and electrical industry, cosmetics and cosmoceuticals (sunscreens, anti-agers, moisturizer), piezoelectric, high temperature lubricants, flame retardant, dental cement, photocatalytic decontamination, solar cell electrodes, paint pigments

Source: Mudunkotuwa, I. A.; Grassian, V. H., The devil is in the details (or the surface): impact of surface structure and surface energetics on understanding the behavior of nanomaterials in the environment. *Journal of Environmental Monitoring* **2011,** 13, (5), 1135-1144.

biomedical applications, pigments, coatings, cosmetics and electronics.[3] Mudunkotuwa

et.al summarizes the applications of metal and metal-based nanomaterials as indicated in the Table 1.1.[3]

Almost all of these functions of nanomaterial have recruited the unique properties of them, derived from their very small size. Klabunde and co-workers have attributed the increased reactivity of nanoparticles to the increased number of edge and corner sites.[4] This can be explained in terms of a cube of which the edge length and the corner sited will increase upon division in to smaller cubes (Figure 1.1). For any given particle, the total free energy can be given as:

$$G_{particle} = G_{bulk} + G_{surface} \qquad \text{Eq. 1}$$

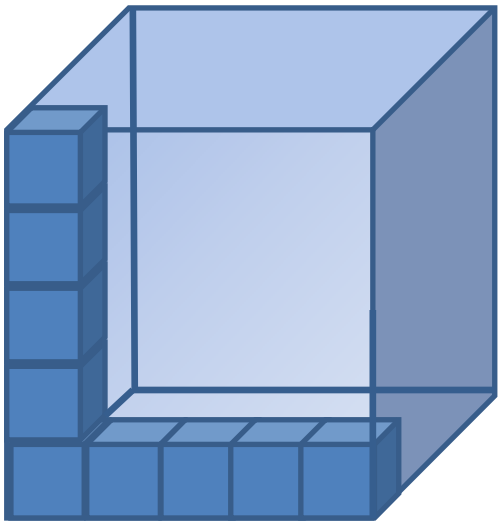

Figure 1.1. The number of edge and corner sites increases with decreasing size: A one 5 cm x 5 cm cube has length of edges = 60 cm and one hundred and twenty five 1 cm x 1 cm cubes have length of edges = 1500 cm (25 times greater)

Source: Grassian V. H., Size-Dependent Properties and Surface Chemistry of Oxide-Based Nanomaterials in Environmental Processes. In *Nanoscale Materials in Chemistry: Environmental Applications*, American Chemical Society: 2010; Vol. 1045, pp 15-33

As a result of increased number of surface atoms, the $G_{surface}$ is in the orders of that of G_{bulk} for the nanoparticles.[3] This large surface free energy of the nanoparticles makes them highly reactive.

1.2 Nanotechnology and the Environment

With the widespread use of metal and metal based nanomaterials, the release of these nanomaterials into the environment during their product life cycle is inevitable. This makes it more likely that increasing human and environmental exposure to nanoparticles will occur. A study done by Kaegi *et.al* in 2008 reports the release of synthetic TiO_2 nanoparticles from urban applications to the aquatic environments.[5] Further, Zheng *et.al* reports the presence of inhalable anatase nanoparticles in the atmosphere and its significance.[6] On the other hand, the potential health risks both to human and to other animals from engineered nanomaterials, is of great interest in many other discussions.[2,7-9] Consequently, the research on identifying the potential environmental and health impacts of engineered nanoparticles has been a hot topic for many researchers. The review by Mudunkotuwa *et.al* summarizes several studies on environmental, health and safety impacts of metal-based nanomaterials.[3]

Once entered into the outer environments, they can exist as atmospheric aerosols or can enter into the aqueous environments. The environmental variables such as pH, temperature, ionic strength and organic matter can have a direct effect for the distribution of nanomaterial in these environments. In aquatic bodies, again nanoparticle can take

different forms; they can exist as dissolved ions, isolated nanoparticles or as aggregates (Figure 1.2).[10]

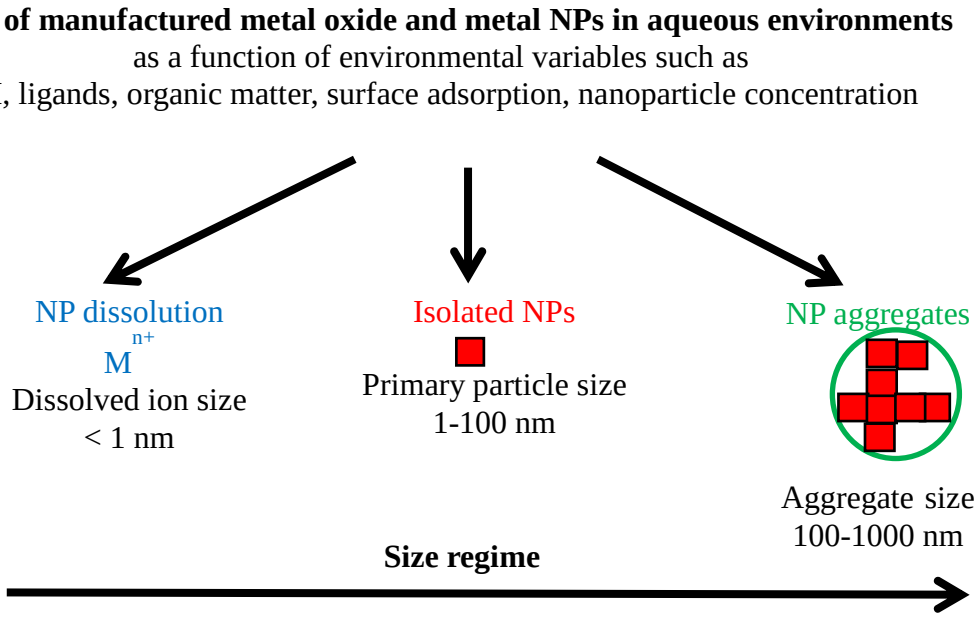

Figure 1.2. The distribution of nanomaterial in aquatic environments

---

Source: Grassian, V. H., When Size Really Matters: Size-Dependent Properties and Surface Chemistry of Metal and Metal Oxide Nanoparticles in Gas and Liquid Phase Environments. *The Journal of Physical Chemistry C* **2008,** 112, (47), 18303-18313.

Because the physical form of nanoparticles in the aquatic environments spans a large range, research on this area requires high attention on selectivity and sensitivity of the techniques.

1.3 Cerium Oxide Nanomaterial

Cerium oxide (ceria), CeO_2, is an important rare-earth metal oxide which adopts a fluorite-type crystal structure, thereby having eight oxygen atoms surrounding each cerium metal cation in the lattice (Figure 1.3).[11,12] Currently, nanoceria, i.e. ceria particles on the nanoscale, is used in a wide variety of applications due to its distinct properties derived from its smaller size, large specific surface area and greater reactivity/activity. Many of these interesting applications utilize the low redox potential of the Ce^{IV}/Ce^{III} redox couple, high oxygen storage ability and the UV absorbing properties of ceria.[13]

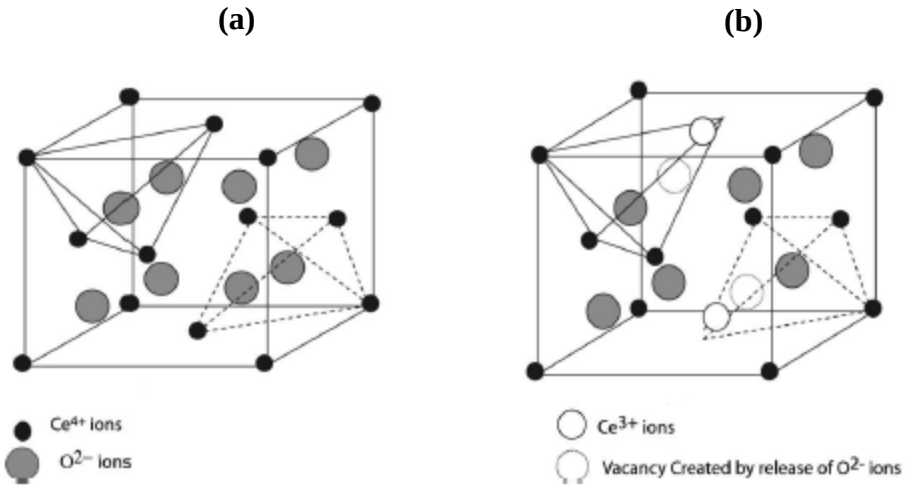

Figure 1.3. The crystal structure of (a) CeO_2 and (b) the distorted crystal structure due to oxygen vacancy creation

Source: Sameer, D.; Swanand, P.; Satyanarayana, V. N. T. K.; Sudipta, S., Size dependency variation in lattice parameter and valency states in nanocrystalline cerium oxide. *Applied Physics Letters* **2005,** 87, (13), 133113.

Furthermore, ceria is being used in solid oxide fuel cells as an electrolyte material, a supporting material in three-way catalysts, in optical coatings, in high storage capacitor devices, as well as components of semiconductors and superconductors.[11,14,15] Biomedical applications of nanoceria are also of great interest and Vladimir et al. provide a good review on this topic.[16] Thus the commercial synthesis of nanoceria has increased in the world during past few years.[17]

Although, the production of ceria nanoparticles has increased, their environmental and toxicological impacts remain unclear and sometimes controversial.[17, 18] Shang *et.al* have recently shown that the nanoceria can induce reactive oxygen species (ROS) accumulation and oxidative damage in *Caenorhabdtis elegans* thereby leading to a decreased lifespan.[18] On the contrary, an earlier study by Xia *et.al* has identified ceria as a suppressor of ROS production and also an inducer of cellular resistance.[19]

Several other studies report on the fate and effect of nanoceria with different sizes in aquatic toxicity tests,[13] effect of surface charge on nanoceria on protein adsorption and cellular uptake of cerium oxide nanopartilces,[20] as well as change in their biological activity when using coating materials and adsorbates from cell culture media.[21] Limbach *et.al* reports on the agglomeration and a quantification of CeO_2 nanoparticle uptake into human lung fibroblasts.[22] Cornelis et.al have recently reported the solubility and the batch retention of CeO_2 nanoparticles in soils.[17]

The fate of metal oxide nanomaterials in the environment depends on a number of factors including pH, temperature, ionic strength and organic matter. Because adsorbed organic acids can alter the surface chemistry of the nanoparticles, organic acid adsorption studies on nanoparticles are of interest so as to better understand the environmental fate

these very small particles. In fact adsorption studies of organic acids such as formic, citric, oxalic, adipic, malonic and succinic have been reported for a number of other metal oxide nanoparticles[23-31], such studies related to nanoceria remain sparse. Sehgal *et.al* reports the use of poly(acrylic acid) to make stable sols of otherwise unstable cerium oxide dispersions.[32] They report on the structure and dynamics of cerium oxide nanosols and their hybrid polymer, investigated by static and dynamic light scattering, X-ray scattering and chemical analysis. Fresnais and coworkers have shown the kinetically mediated naoceria-poly(acrylic acid) cluster formation.[33]

1.4 Scope of the Study

The study described herein focuses on the adsorption of citric acid on commercially available cerium oxide nanoparticles at circumneutral and acidic pHs. Citric acid, an important biologically and environmentally relevant ligand, is a tricarboxylic acid with pK_{a1} = 3.13, pK_{a2} = 4.76 and pK_{a3} = 6.40 (Figure 1.4). In addition to its natural abundance, citrate is a common stabilizer used in the synthesis of CeO_2 nanoparticles.[34-38] Further, citrate species are important as coatings on nanomaterials for their biological applications too. Safi *et.al* reports the enhanced adsorption of citrate coated ceria nanoparticles by NIH/3T3 mouse fibroblasts.[34] In addition, Cornelis *et.al* reports the effect of citric acid on zeta potential and the hydrodynamic diameter of CeO_2 nanoparticles.[17] However, to date, studies on citric acid speciation on nanoceria in aqueous phase have not been reported.

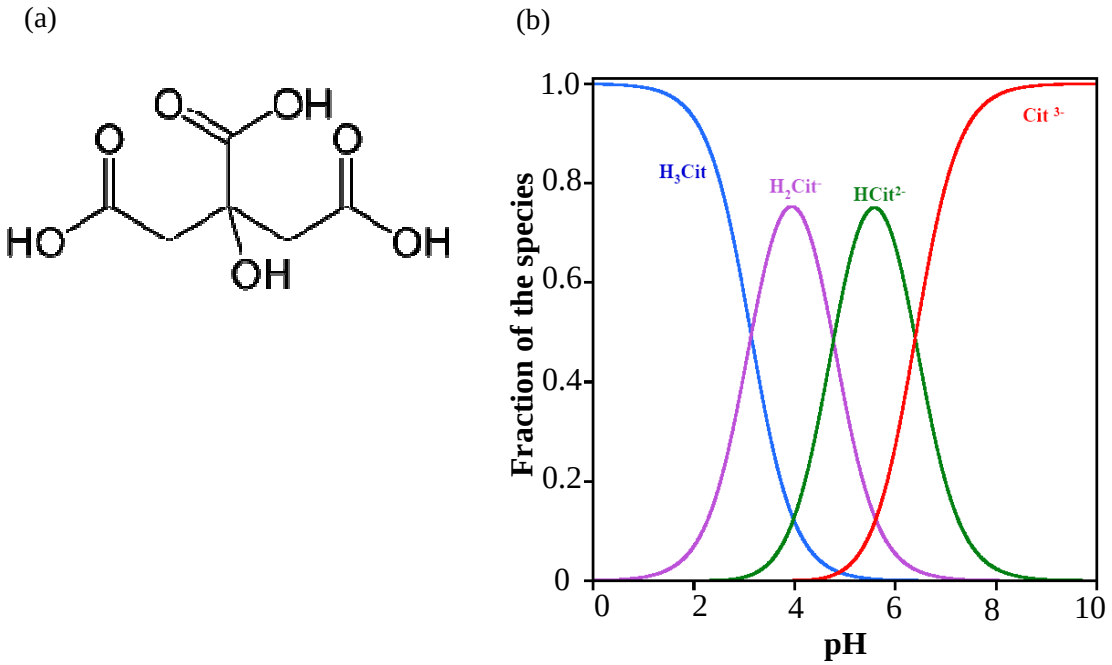

Figure 1.4. Citric acid (a) Structure and (b) Calculated speciation as a function of pH

A variety of techniques are currently in use to detect the behavior of nanomaterial in different environments. The outline for this study is summarized in Figure 1.5. In this study, the adsorption of citric acid has been investigated with an emphasis on particle size effects using ATR-FTIR spectroscopy to probe surface speciation and quantitative solution phase adsorption measurements to determine surface coverage. The thermodynamic considerations predict higher organic acid adsorption on smaller particles.[24] However, the variation in the mode of adsorption of organic acid with particle size will also be important in quantitative determinations and which is another main

concern in this study. In addition, the aggregation of nanoceria is probed qualitatively by observing the sedimentation patterns using UV-Vis spectroscopy.

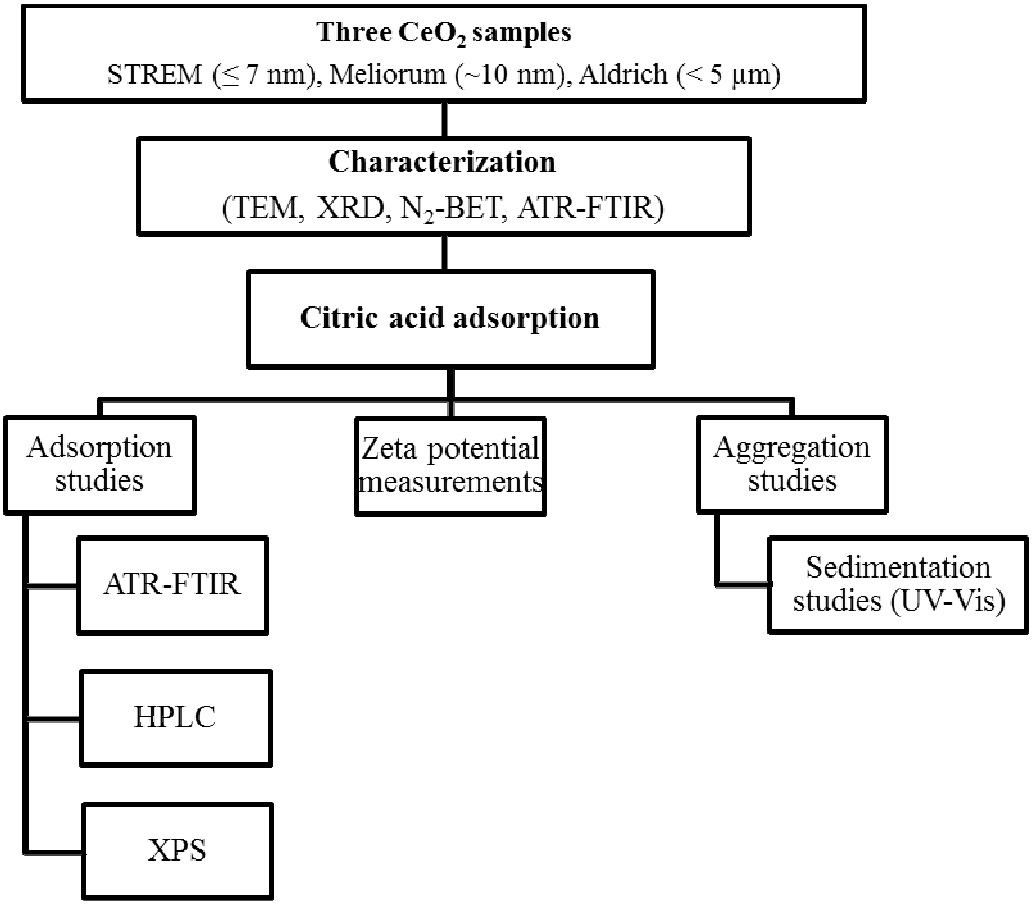

Figure 1.5. Outline of the research

CHAPTER 2

EXPERIMENTAL PROCEDURE

2.1 Reagents

All experiments were conducted with commercially purchased CeO_2 nanoparticles from STREM chemicals (≤7 nm, manufacturer's specified), Meliorum (~10 nm, manufacturer's specified) and Sigma Aldrich (<5 μm, manufacturer's specified). Solution phase studies were conducted using solutions of 2-(n-morpholino)ethenesulfonic acid (MES; Sigma Aldrich; ≥ 99%), 4-(2-hydroxyethyl)-1-piparazeneethanesulfonic acid (HEPES; Sigma Aldrich, ≥ 99.5%), or hydrochloric acid (HCl; Fisher Scientific; certified ACS plus). To adjust the pH of the solutions, sodium hydroxide (NaOH; Fisher Scientific; certified ACS plus) was used. To keep the solution ionic speciation at minimum, sodium chloride (NaCl; Fisher Scientific; certified ACS plus) was used to adjust ionic strength. The aqueous solutions of citric acid (Sigma Aldrich, 99.5% certified ACS plus) and all reactors were prepared using Optima water (Fisher Scientific).

2.2 Purification of STREM CeO_2 Sample

In order to remove the organic impurities indicated by the ATR-FTIR spectra of STREM CeO_2 sample, several purification methods were carried out. First attempt was to purify the sample by calcination. Calcination of STREM CeO_2 sample was done at several different conditions: 393 K/2 hours; 393 K/overnight; 673 K/overnight and 1123 K/overnight. After that the purification was done by washing the sample by 1 M HCl and

oven drying at 393 K overnight. The acid washing procedure was optimized by varying the sonication time period and duration of mixing. The 4 nm sample described herein refers to the STREM CeO_2 sample washed by 1 M HCl and oven dried at 393 K overnight.

2.3 Characterization of Bulk and Surface Properties of CeO_2 NPs

Bulk particles properties of crystallinity and size were characterized with powder X-ray diffraction (XRD) and the analysis of transmission electron microscopy (TEM) images. XRD patterns were collected using a Rigaku Miniflex II diffractometer with a Co source and a Fe filter, to determine crystalline phases present for nanoceria samples as a function of size. TEM images were collected using JEM JEOL-1230 microscope, operated at 120 kV. Samples were suspended in methanol or water prior. From those suspensions one or two drops were dried on to a copper grid with holey amorphous carbon film. For particle size distributions, digital images were acquired using a Gatan UltraScan CCD camera with Gatan imaging software. The size of the ceria particles was then determined by analyzing TEM images using ImageJ. Particle size distributions were determined from the analysis of hundreds of particles (250 – 500 particles) for each sample. The 39 nm particles were imaged by S-4800 scanning electron microscope. The suspension prepared in methanol was placed on a Si wafer which was then stuck on aluminum stub.

Nanoceria surfaces were analyzed for surface composition and surface area. For surface area, a seven-point nitrogen-BET adsorption isotherm apparatus (Quantachrome

4200e surface area analyzer) was used to determine the specific surface area of nanoceria. Samples were degassed at 393 K overnight (~16 h) prior to the analysis. In addition to the experimentally measured BET specific surface areas, the geometric surface area of each particle size was estimated using a CeO_2 density of 7.21 g/cm^3 [17] and assuming a spherical particle morphology. Surface composition and cerium oxidation states were measured using a custom-designed Kratos Axis Ultra X-ray photoelectron spectroscopy system. High resolution spectra were acquired in Ce, O, C and S regions using 20 to 40 eV energy window; pass energy of 20 eV; step size of 0.1 eV and dwell time of 1000 ms.

2.4 ATR-FTIR Spectroscopy

Surface adsorption studies were done using an Attenuated Total Reflectance Fourier Transform Infrared (ATR-FTIR) spectroscopy. ATR-FTIR data for citric acid adsorption on nanoceria were recorded at pH values: 2.0, 4.0, 5.5 and 7.5 using a Thermo-Nicolete FTIR spectrometer equipped with a MCT/A detector. Solution phase measurements in the absence of nanoceria were also recorded so as to compare solution phase speciation to that for the nanoceria-citrate complex. For solution phase measurements, an ATR-FTIR spectrum was recorded using 100 mM citric acid solutions at the four pH values. Surface adsorption on to CeO_2 surface was measured using a thin, evenly coated nanoceria films prepared by placing a suspension of nanparticles (~10 mg in 1 mL of optima water) onto an AMTIR crystal element in a horizontal ATR cell (Pike Technologies, Inc.). The suspension was allowed to dry overnight prior such at a thin film was formed and subsequently used for surface adsorption measurements. After

recording the nanoceria spectrum, 1.0 mM citric acid solution at selected pH (2.0, 4.0, 5.5 and 7.5) was placed on the thin film of CeO_2 and spectra were recorded for 1h in 10 min intervals (Figure 2.1). 150 scans were recorded at an instrument resolution of 4 cm^{-1}. Spectra for adsorbed citrate were obtained by subtracting out the spectrum of the nanoceria surface and water vapor.

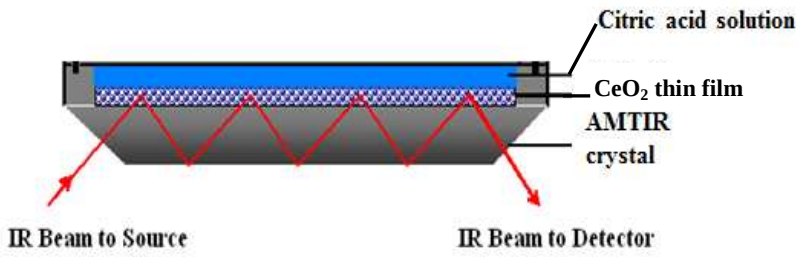

Figure 2.1. Sample preparation on AMTIR crystal

In order to understand some bands appeared upon citric acid adsorption on nanoceria, the adsorption studies were carried out using acetic acid, which is a much simpler acid. The adsorptions studies were conducted using 1 mM acetic acid at pH 2.0 and 7.5, using the same method described for citric acid.

2.5 Quantitative adsorption measurements

Solution phase adsorption studies were conducted in aqueous batch reactors at pH 2.0, 4.0, 5.5 and 7.5. Solutions at pH 2.0 and 4.0 consisted of 0.01 and 0.0001 N HCl

solutions, while solutions at pH 5.5 and 7.5 consisted of 25 mM of MES and HEPES, respectively, for pH control. A NaOH solution (8 M) was used to adjust pHs of higher pH solutions. All the solutions were prepared to have an ionic strength of 0.03 M NaCl, because of the ionic strength of pH 2.0 solution. The adsorption experiments were conducted as follows. Stock solutions of 10 mM citric acid were prepared at pH 2.0, 4.0, 5.5 and 7.5 at 293 K. Reactors in the concentration range of 0.1 – 10 mM were prepared from these citric acid stock solutions, diluting in the appropriate buffer of each pH. In order to quantify the initial citric acid concentration, 1 mL of the sample was drawn out from each vial, prior to the addition of the solid. A CeO_2 solid loading of 2.0 g/L in the reactors was used. After mixing the solid, the sealed reactors covered with aluminum foil were mixed on a Cole-Parmer circular rotor for 24 h. The suspension pH was measured after completion of the mixing. An aliquot of 1 mL of solution drawn out from each reactor was passed through a 0.2 µm syringe-driven filter (Xpertec) into separate centrifugation vials, and centrifuged at 14000 rpm for 1 hour to remove CeO_2 particles from the solution. Filtered samples were analyzed using a Dionex Ultimate 3000 HPLC that was equipped with a diode array detector at 226.0 nm and used optima water mobile phase, of which pH has been adjusted to 2 using conc. $HClO_4$. The instrument response was measured with respect to citric acid standards, which were made fresh for each set of reactors. The concentration of adsorbed citric acid was then determined using the difference of the initial and final concentrations measured for each experimental system.

2.6 Nanoparticle-nanoparticle interactions, zeta potential and aggregation measurements

Sedimentation experiments were used to probe the nanoparticle-nanoparticle interactions and the aggregation behavior, in which the changes in light scattering were measured as a function of time when passing through CeO_2 suspensions (1.0 g/L). The suspensions prepared were placed in 1 cm path length cuvette and the amount of transmitted light was measured by a UV-Vis spectrophotometer at a wavelength of 510 nm. The sonicated (1 min) suspensions were left overnight to reach steady state equilibrium, thereby assuming no aggregation happens during the measurements. Thus the sedimentation pattern observed can be attributed only to the gravitational settling down of the particles depending on their particle or aggregate size.

The surface charge of nanoparticles was measured using the zeta potential mode of the Beckman Coulter Delsa Nano C instrument. All suspensions were prepared to have a solid loading of 1.0 g/L, 1 mM of citric acid, and a fixed ionic strength of 0.03 M. The suspensions were sonicated (Sonics-Vibra cell ultrasonicator) for 2 min after mixing. Measurements were made at pH 2.0, 4.0, 5.5 and 7.5. These experiments were also conducted in the absence of citric acid.

2.7 X-ray photoelectron spectroscopy

In addition, the quantification studies were carried out using XPS as well. Cerium oxide samples with a solid loading of 2.0 g/L were suspended in 10 mM citric acid

solution at pH 2.0 and 7.5 with a constant ionic strength of 0.03 M and allowed to equilibrate for 24 hours. The citric acid adsorbed cerium oxide samples were separated, washed with optima water, dried in a lyophilizer and were scanned for the Ce, C and O regions using the custom-designed Kratos Axis Ultra X-ray photoelectron spectroscopy system described by Baltrusaitis *et.al*.[39, 40]

CHAPTER 3

RESULTS AND DISCUSSION

3.1 Purification of 4 nm nanoceria sample

A comparison of results from all the purification methods followed for the 4 nm nanoceria sample is indicated in Figure 3.1 in terms of a comparison of ATR-FTIR spectra. Calcination of the sample at temperatures below 773 K did not show any considerable removal of the impurity, which is evidenced by the unchanged ATR-FTIR spectra around 1500 cm^{-1} region.

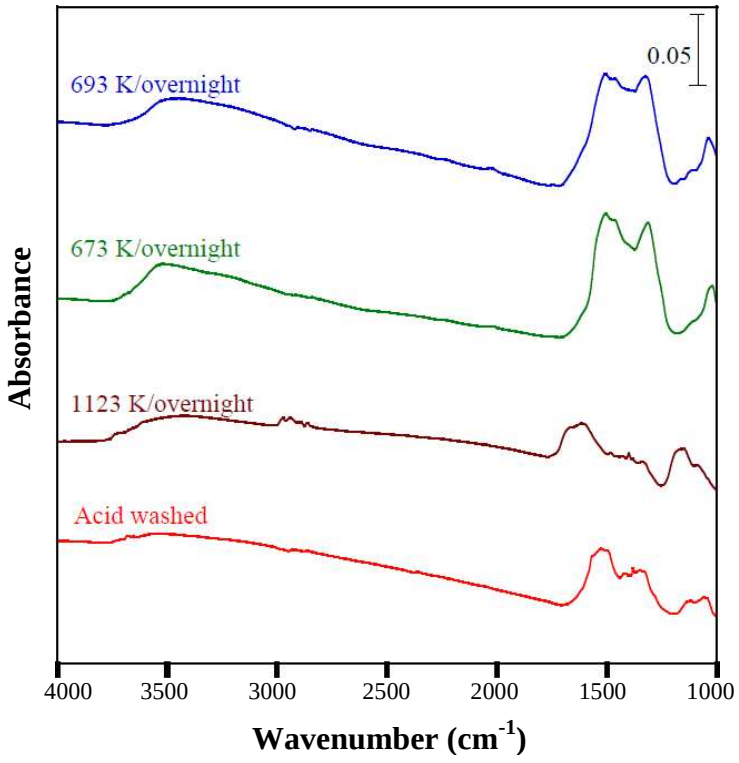

Figure 3.1. Comparison of purification methods for 4 nm CeO_2

Even though, the calcination at 1123 K seems to remove some amount of the organic impurity, exposure to such high temperatures seems to cause the sintering of these very small nanoparticles. This is evidenced by the change in the color of the nanoparticles from light yellow to pink (Figure 3.2). However, the acid washed 4 nm CeO_2 did not show any such physical change in the particles. The 4 nm CeO_2 nanoparticles referred to from here onwards are the acid washed CeO_2 nanoparticles.

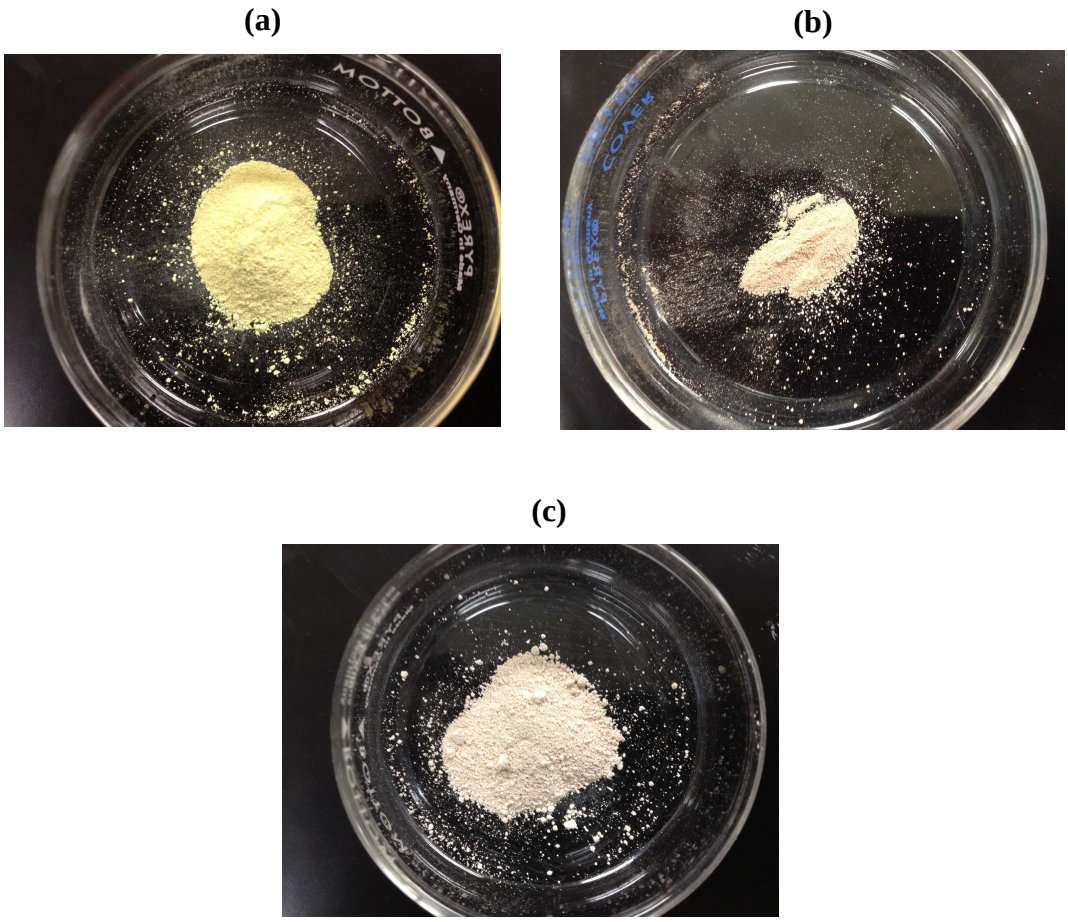

Figure 3.2. Colors of (a) Acid washed 4 nm CeO_2 (pale yellow) (b) Calcinated CeO_2 at 850 °C (pink) (c) 39 nm CeO_2 sample (pale pink)

3.2 Characterization of Three Different Sized Nanoceria Samples

A summary of the physicochemical characterization data for three different nanoceria samples is given in Table 3.1.

Table 3.1. Summary of CeO_2 nanoparticle (nanoceria) samples: Bulk and surface properties including size, surface area and percent Ce(III)

Physicochemical Property	Commercial Source		
	STREM	Meliorum	Aldrich
Primary particle size[a] (diameter (nm))	4.3±1.5	8.7±3.7	39±32
Measured BET surface area (m^2/g)	80±7	62±8	5.6±0.2
Calculated geometric surface area (m^2/g)	197±69	96±41	21±14
% Ce(III) from XPS	21	14	12

[a] Based on TEM images

The XRD and TEM data show that these three different nanoceria samples have different sizes. The XRD results are in agreement with those reported previously for CeO_2 and confirms the fluorite crystal structure of CeO_2 nanoparticles as shown Figure 3.3.[12, 36, 37] As expected from the Scherrer equation (Eq.2),

$$t = \frac{\kappa \lambda}{\beta \cos\theta} \qquad \text{Eq.2}$$

the full width half maximum (β) is inversely proportional to crystallite size (t). Other parameters in Eq. 2 include the shape factor (κ), wavelength of X-ray (λ), and Bragg angle (θ). The XRD peaks are in fact broadened with decreasing particle size as determined by TEM.

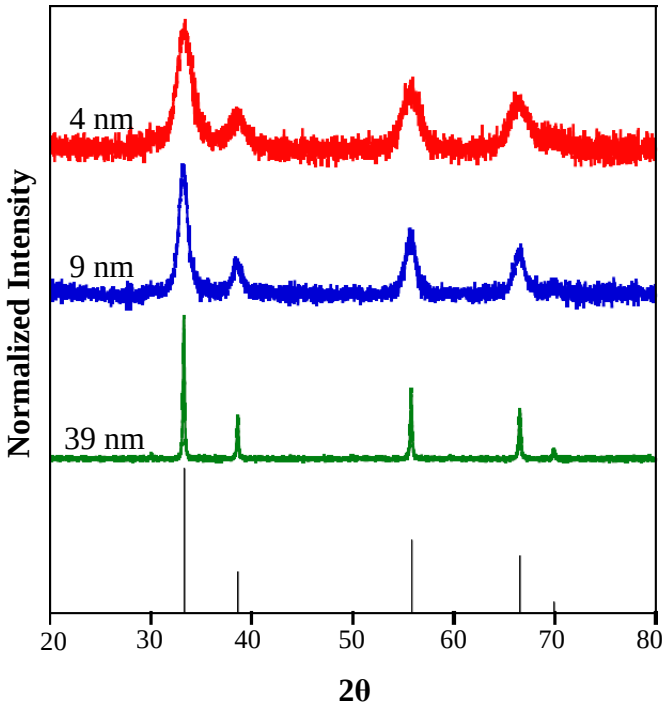

Figure 3.3. Powder X-ray diffraction patterns of 4 nm, 9 nm and 39 nm CeO_2 Particles compared with a standard XRD pattern for CeO_2.

Analysis of TEM images for these three samples showed that the nanoparticle diameters have mean values of 4, 9 and 39 nm (Figure 3.4) which are also included in Table 3.1. Even though the Aldrich nanoceria sample has an average particle diameter of 39 nm, it

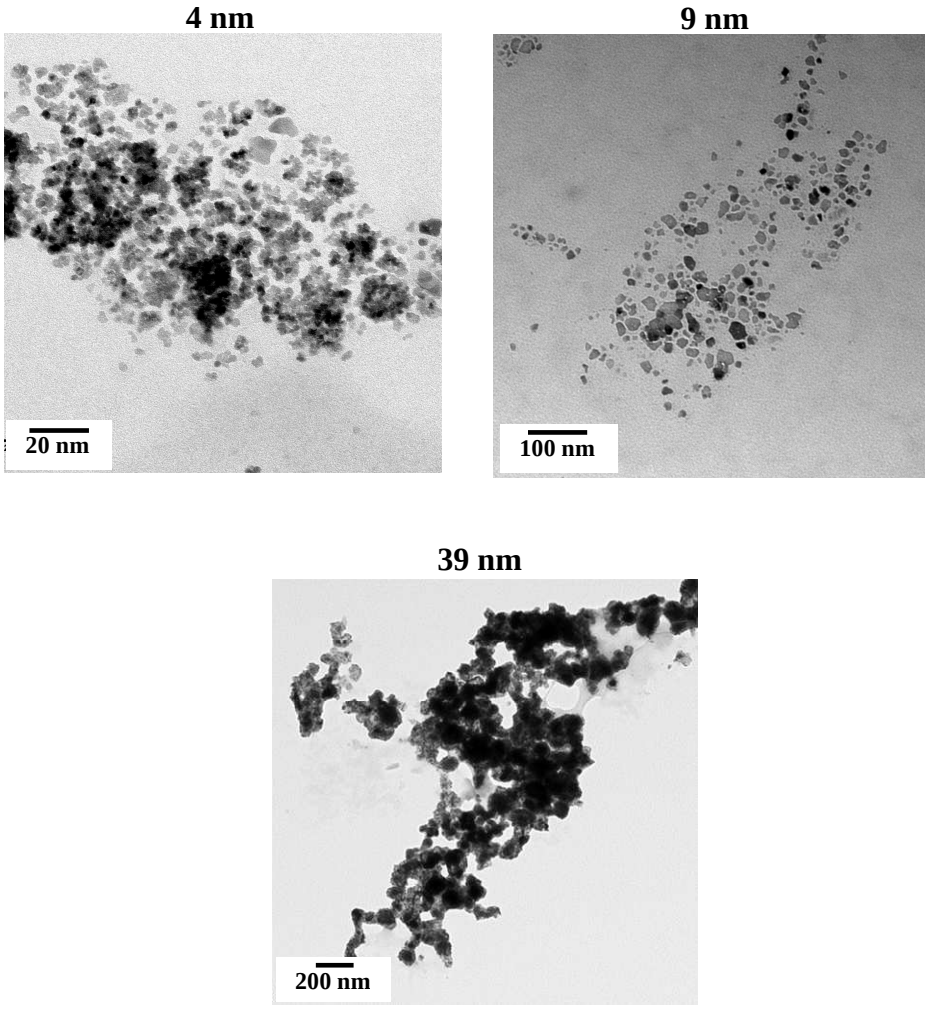

Figure 3.4. TEM images of CeO_2 nanoparticles of different size: 4 nm, 9 nm and 39 nm.

consists of CeO_2 nanoparticles with a wide size distribution compared to other two samples (see Figure 3.5).

The measured seven-point BET surface areas were 80±7, 62±8 and 5.6±0.2 m^2/g for 4, 9 and 39 nm samples respectively, where uncertainties represent the standard deviation of four measurements, are found to decrease with increasing particle size.

However, the calculated geometric surface areas are much different: 197±69, 96±41 and 21±14 m^2/g for 4, 9 and 39 nm particles respectively. These differences between geometric and N_2-BET surface area values are mainly due to the fact that not all of the available surface area is available for adsorption due to nanoparticle aggregation which

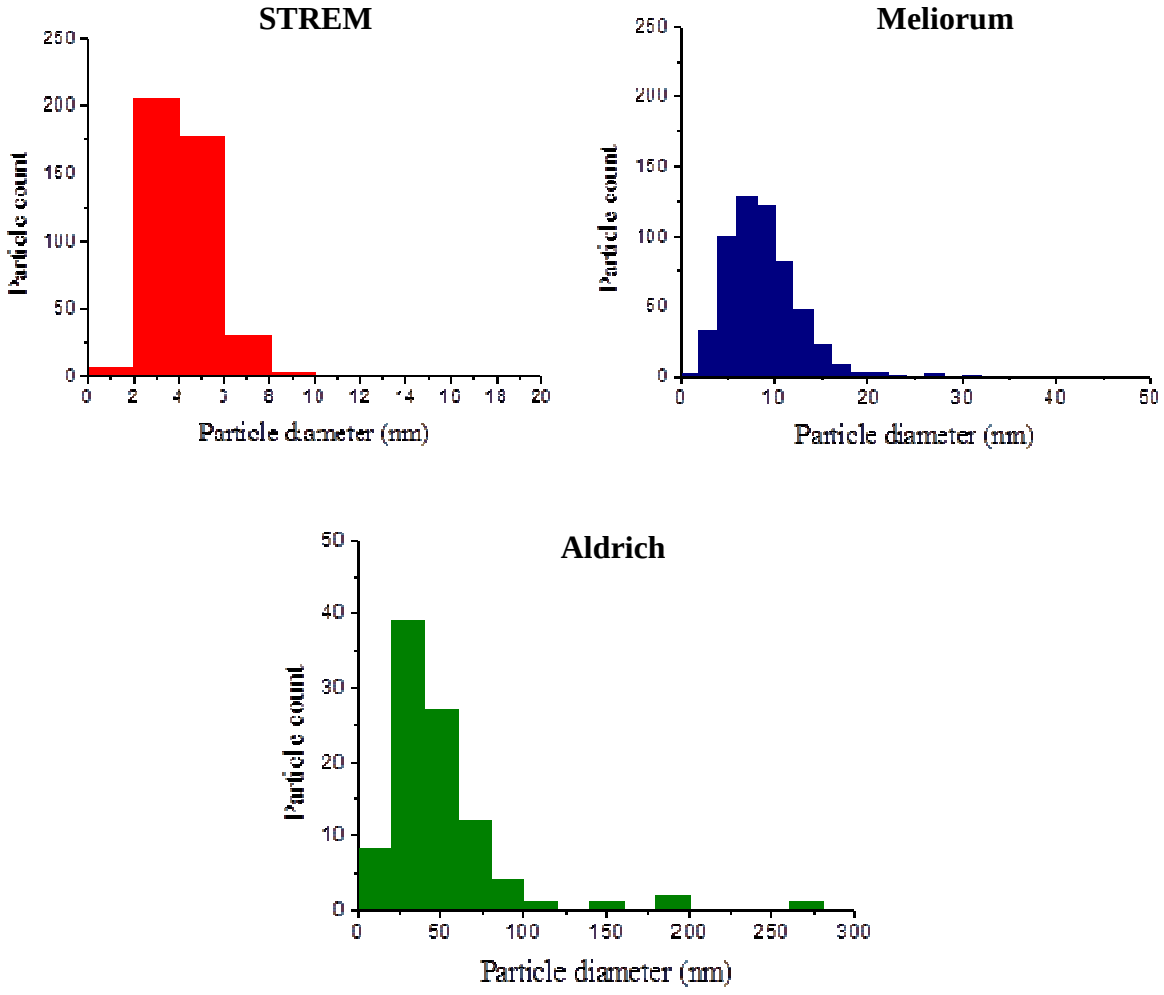

Figure 3.5. Particle size distributions of three CeO_2 nanoparticle samples

limits the available surface area. The SEM analysis of 39 nm particles evidences for the aggregation of these nanoparticles (Figure 3.6). Additionally, any deviation of particle geometry from spherical shape can also account for differences between these two values.

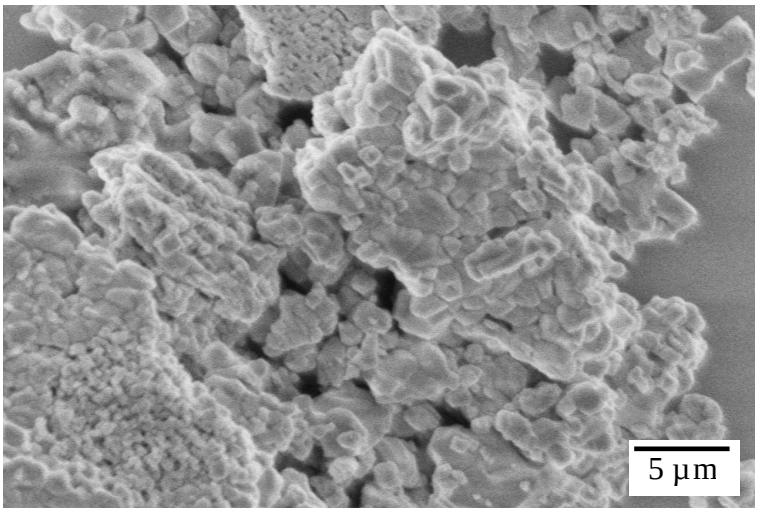

Figure 3.6. SEM image of 39 nm CeO_2 nanoparticles

XPS data for all three samples show there is a mixture of both Ce^{3+} and Ce^{4+} oxidation states in the near surface region (Figure 3.7) as reported in other studies on ceria.[12] Even though, the C 1s XPS spectra of 4 and 9 nm ceria have similar patterns showing a very minute amount of organic carbon, that of 39 nm shows the presence of relatively higher amount of carbon species (Figure 3.7). This may be due to an organic coating on these nanoparticles or some left over organic precursor used in the synthesis. The O 1s spectra for three samples are similar to each other are also shown in Figure 3.7.

The relative abundances of each oxidation state of ceria has been shown to be a function of particle size.[12, 41] From the XPS data, the calculated percentages of Ce^{3+}

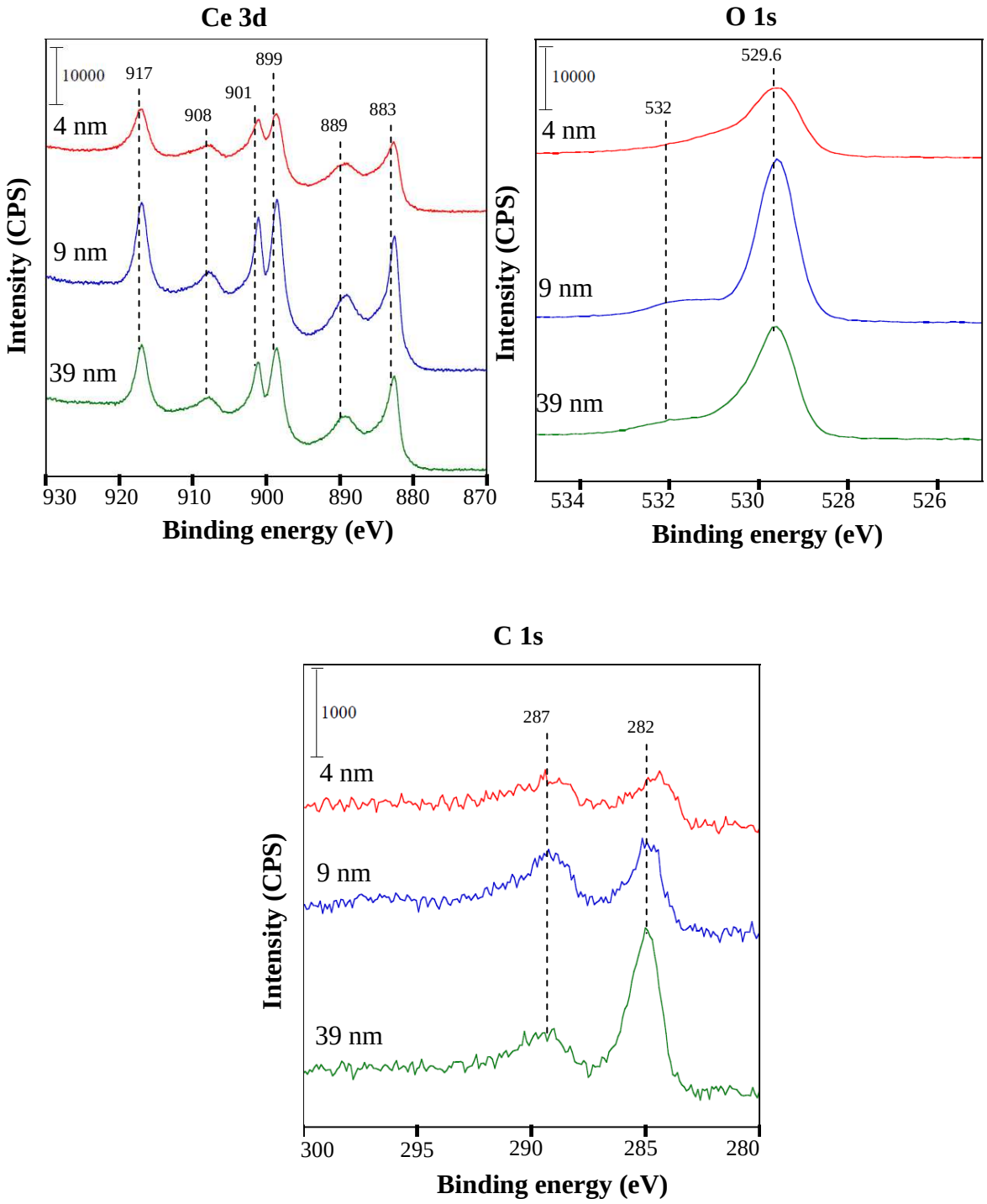

Figure 3.7. X-ray photoelectron spectra of 4 nm, 9 nm and 39 nm CeO_2 in the Ce 3d, O 1s and C 1s binding energy regions.

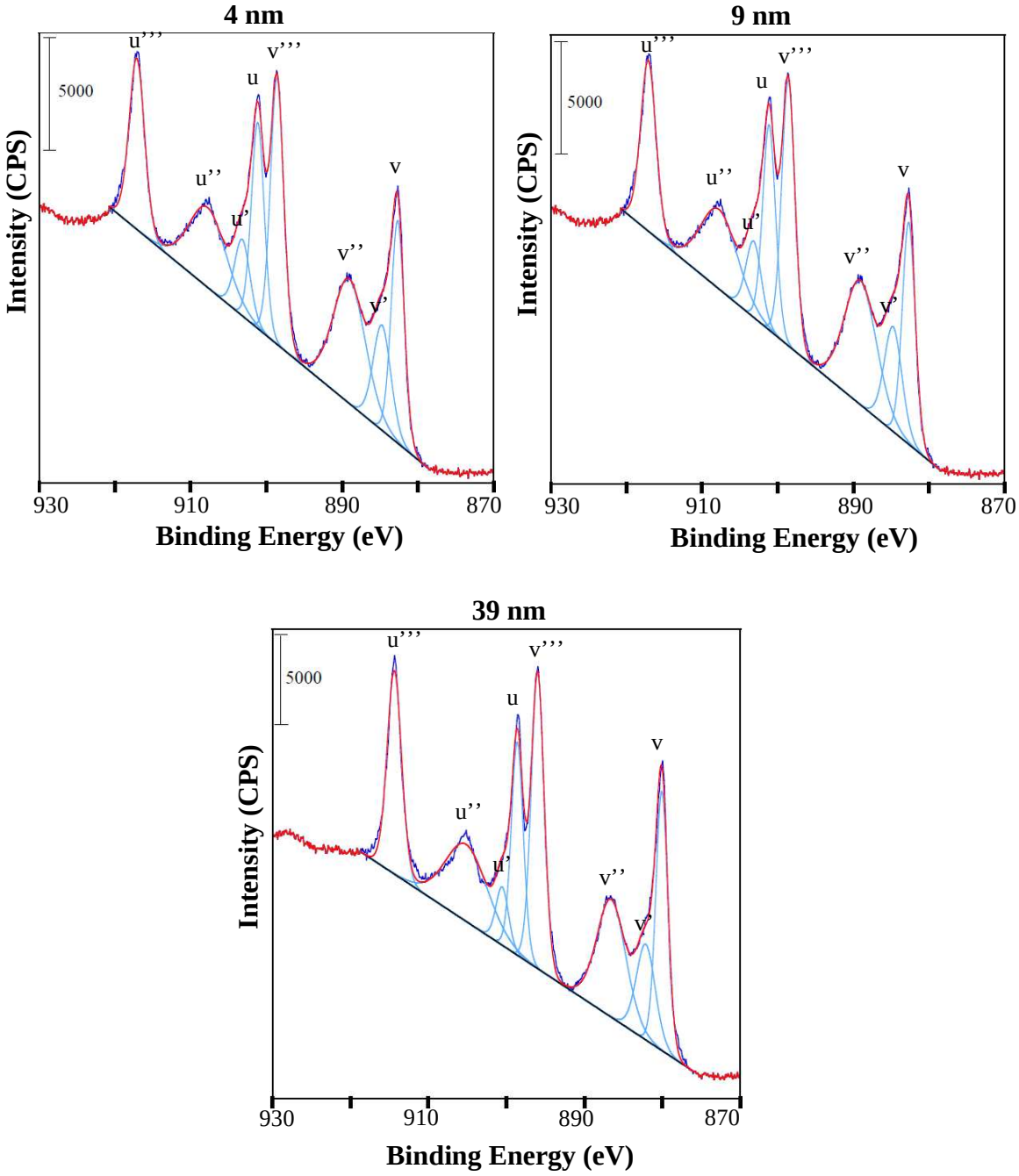

Figure 3.8. Ce 3d XPS spectra of 4nm, 9 nm and 39 nm CeO_2 nanoparticles

oxidation state are included in Table 3.1. The relative amounts of Ce^{3+} and Ce^{4+} can be calculated from XPS data by spectral curve fitting the Ce 3d binding energy region (Figure 3.8). Curve fitting in this binding energy region was done using the procedure outlined in previous XPS studies of cerium oxide and of nanoceria.[42, 43] In particular, the peaks at 903 eV (u') and 885 eV (v') are assigned to the Ce^{3+} oxidation state whereas the peaks at 917 eV (u"'), 908 eV (u"), 901 eV (u) 899 eV (v"'), 889 eV (v") and 883 eV (v) are assigned to cerium in the Ce^{4+} oxidation state.[1,2] Therefore, the Ce^{3+} percentage in the sample, Ce^{3+}%, is calculated using the relative areas under the peaks according to Eq 3:

$$Ce^{3+}\ \% = \frac{Ce^{3+}}{Ce^{3+} + Ce^{4+}} \times 100 \qquad \text{Eq. 3}$$

where Ce^{3+} on the right hand side of the equation represents the total area under the u' and v' bands and Ce^{4+} represents the total area under the u''', u'', u, v''', v'' and v bands. These data show that the smallest nanoparticle has the largest percentage of reduced cerium, in agreement with earlier studies. The comparatively higher amount of Ce^{3+} present in smaller nanoparticles can be attributed to the presence of oxygen vacancies more in smaller CeO_2 nanoparticles than those in larger nanoparticles.[12]

The ATR-FTIR spectra for the three particles are given below, which are important for the citric acid adsorption studies (Figure3.9). Except for the phonon modes observed around 1000 cm^{-1} region and the bands at 3449 cm^{-1} corresponding to hydroxyl groups, 4 nm and 39 nm sample show the bands due to organic impurities in them in the region around 1600 -1400 cm^{-1}.

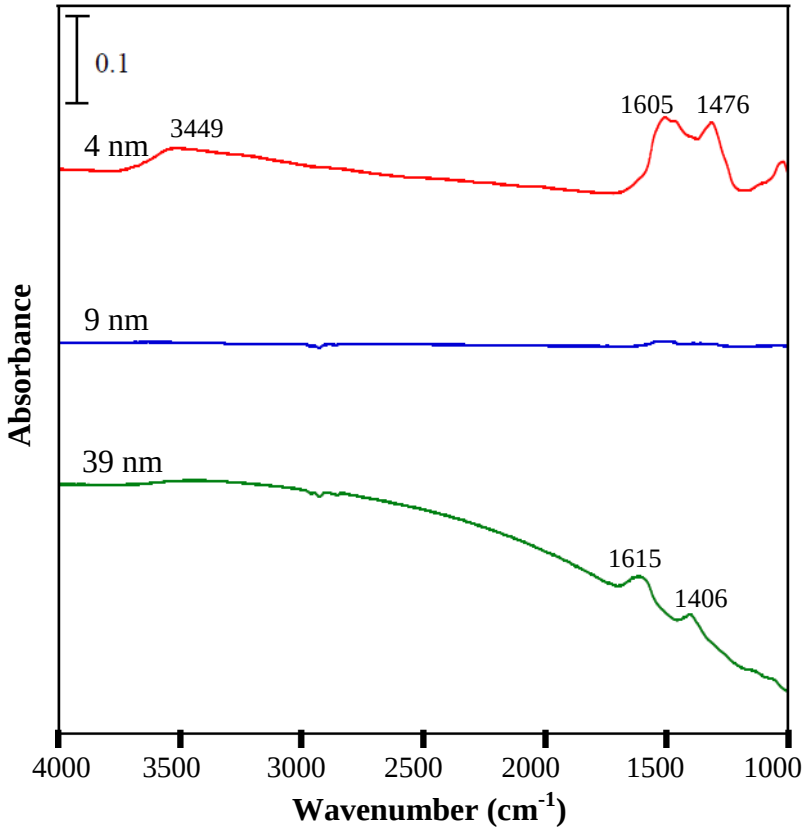

Figure 3.9. ATR-FTIR spectra of 4 nm, 9 nm and 39 nm CeO_2 nanoparticles

3.3 Citric Acid Adsorption on CeO_2 NPs: Spectroscopic Studies

In solution phase, the infrared spectrum for citric acid shows two prominent peaks at 1570 and 1391 cm^{-1} at pH 7.5 (Figure 3.10), which can be assigned to asymmetric and symmetric stretches of carboxylate group respectively.[23-31] There is also a much weaker absorption around 1280 cm^{-1} at this pH that can be assigned to the coupled stretches and bends of carboxylate group.[23] With decreasing pH, these bands diminish in their intensity, while two new bands corresponding to the C=O stretching motion and coupled

C-(OH) and C-O-H bending motions appear at 1722 cm^{-1} and 1226 cm^{-1} respectively.[23, 25, 29, 30] These solution phase spectra confirm the fully protonated structure of citric acid at pH 2.0 and a completely deprotonated structure at pH 7.5. The pH values in between are due to partially protonated structures at pH 4.0 and 5.5, which is consistent with the pK_a values and previous studies.[23]

Table 3.2. Vibrational frequencies (cm^{-1}) and assignments of solution phase and adsorbed citric acid

Wavenumber (cm^{-1})	Assignment
1722	-C=O stretching
1570, 1615	$-COO^-$ Asymmetric stretching
1391, 1370	$-COO^-$ Symmetric stretching
1280	$-COO^-$ Coupled stretching and bending
1226	Couples C-(OH) and C-O-H bending
1432	$-CH_2-$ bending

Spectroscopic measurements as a *f*(pH) gave useful comparison of the citrate-surface adsorbed complex for 4 nm and 9 nm CeO_2 samples. Nanoceria with a particle size of 39 nm did not show any absorption bands in the ATR-FTIR spectroscopy due to the low available surface area for this material and the possibility of the presence of surface impurities from the commercial manufacturing process. ATR-FTIR spectra of the

9 nm CeO_2 particles are shown in Figure 3.11. The main feature of these spectra at all four pHs is that the peak at1722 cm^{-1} observed at low pH solution spectra, which is corresponding to C=O stretching, is absent in the surface adsorbed citric acid complex. This implies that citric acid has adsorbed on to the CeO_2 surface irrespective of the pH,

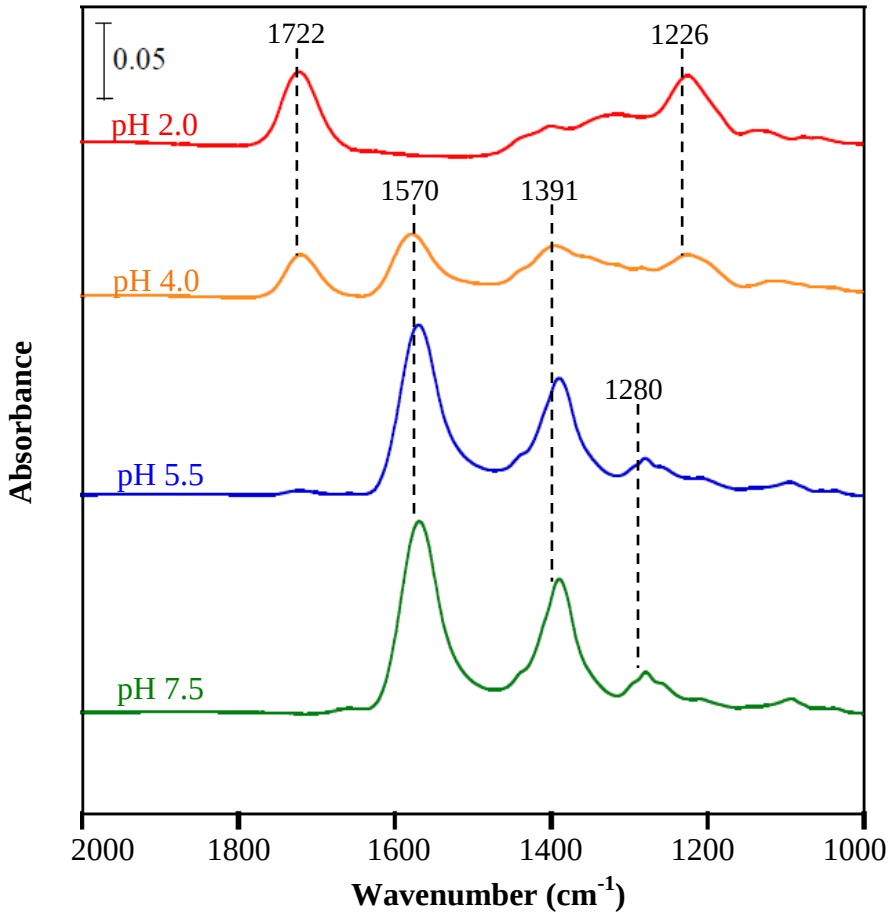

Figure 3.10. ATR-FTIR spectra of 100 mM citric acid solution at different pHs: 2.0, 4.0, 5.5 and 7.5

yielding the fully deprotonated form of citric acid. Further, the two peaks corresponding to asymmetric and symmetric stretches of carboxylate groups can be observed at 1565 and 1396 cm^{-1} respectively. The shoulder around 1432 cm^{-1}, which appears from the beginning and does not show a considerable growth in the time course experiments, is

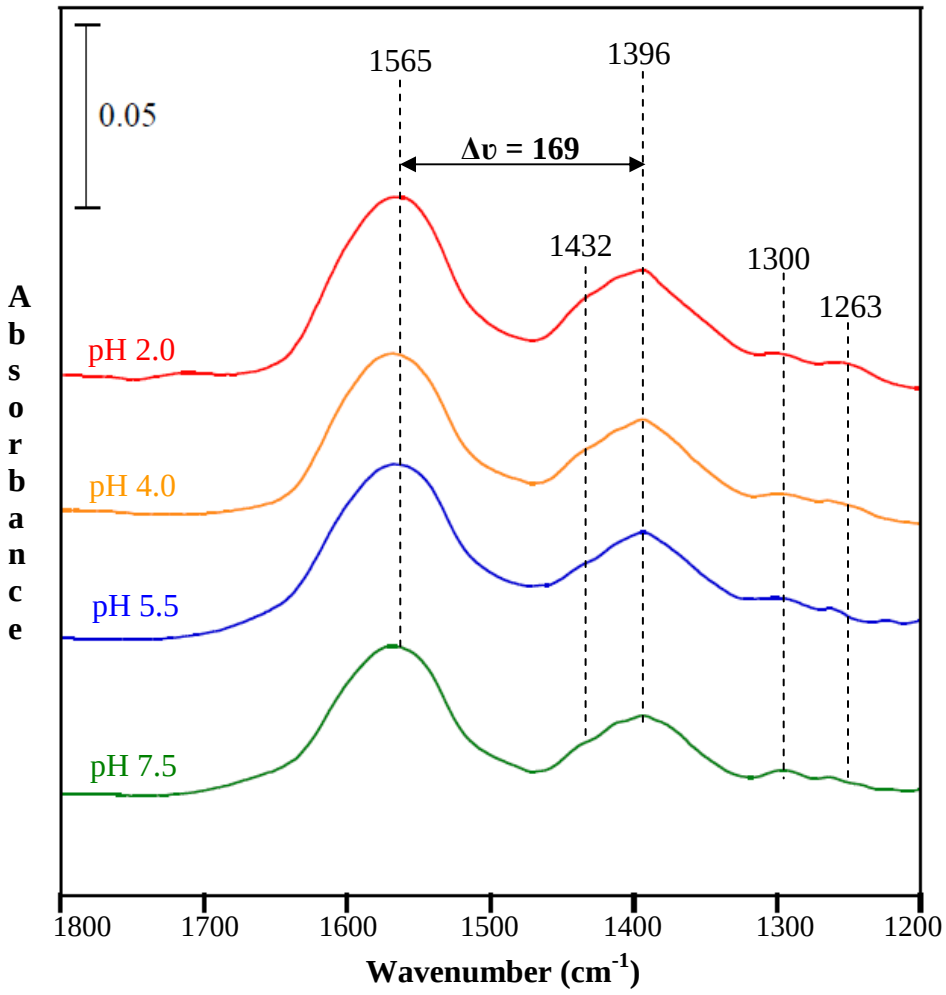

Figure 3.11. ATR-FTIR spectra of adsorbed citric acid on 9 nm CeO_2 at different pHs: 2.0, 4.0, 5.5 and 7.5

attributed to the bending modes of CH_2 groups of adsorbed citric acid.[44] The weaker absorptions at 1300 and 1263 cm^{-1} are due to bending modes of the carboxylate groups.

ATR-FTIR spectra of 4 nm sized nanoceria particles show differences from the larger 9 nm particles and have several interesting features in the spectrum (Figure 3.12).

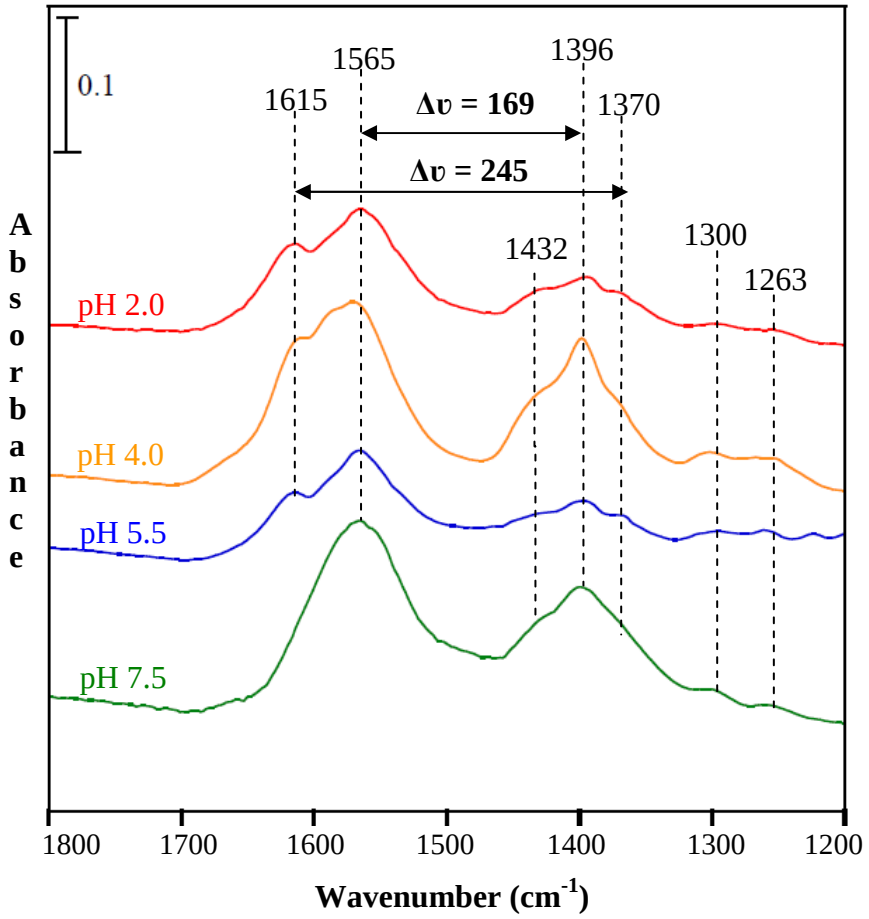

Figure 3.12. ATR-FTIR spectra of adsorbed citric acid on 4 nm CeO_2 at different pHs: 2.0, 4.0, 5.5 and 7.5

First, like 9 nm particles there is no peak at 1722 cm^{-1} in the spectrum which suggests that the fully deprotonated form of citric acid exists for these very smaller nanoparticles

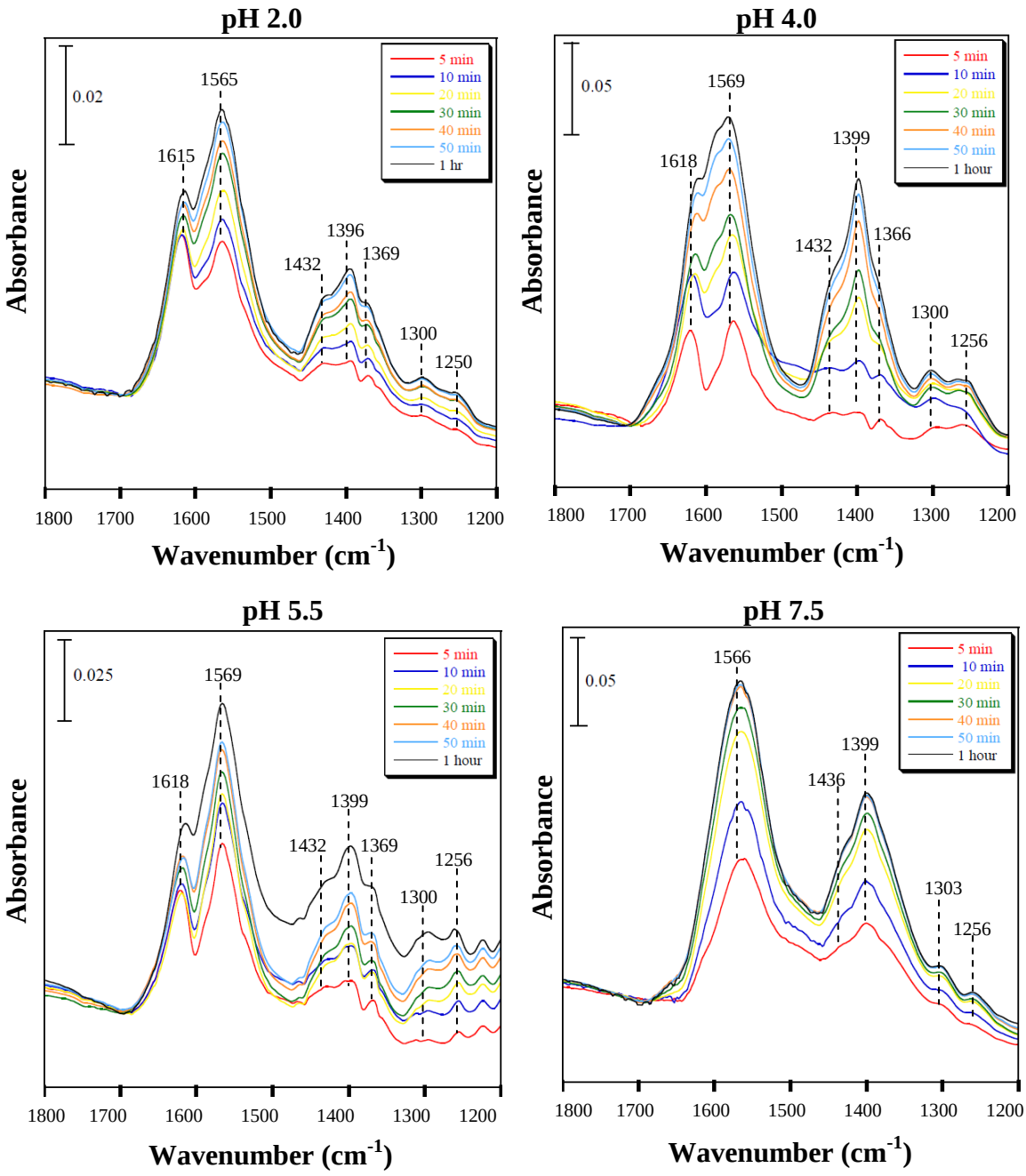

Figure 3.13. ATR-FTIR spectra of adsorbed citric acid on 4 nm CeO_2 as a function of time.

as well. The spectrum of the adsorbed citric acid complex on 4 nm ceria at pH 7.5 is similar to those of 9 nm ceria particles. However, in addition to the three main regions

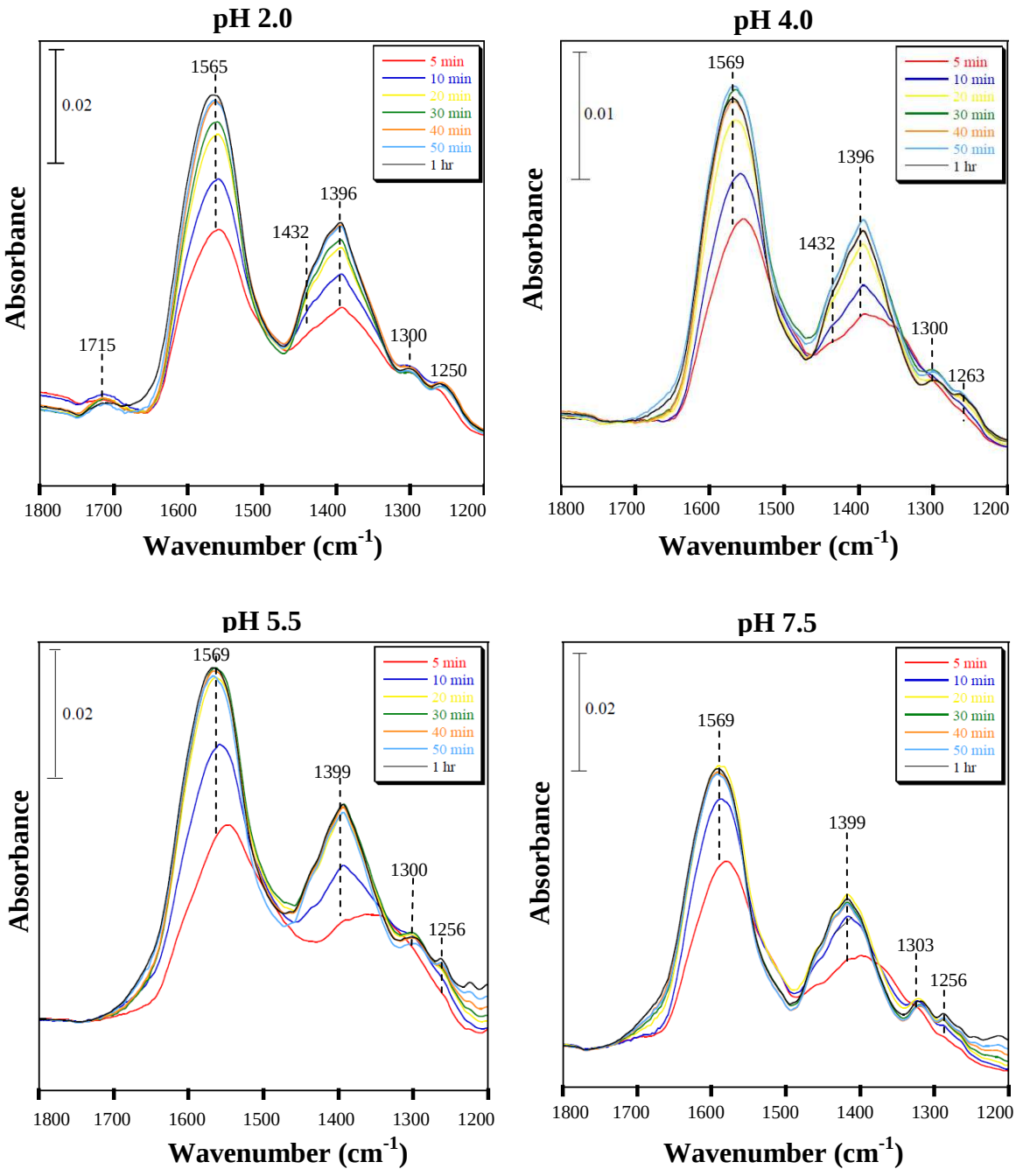

Figure 3.14. ATR-FTIR spectra of adsorbed citric acid on 9 nm CeO_2 as a function of time.

corresponding to asymmetric, symmetric and bending modes of carboxylate group, the spectrum changes and new peaks around 1615 and 1370 cm^{-1} grow in at pH 2.0, 4.0 and 5.5 for 4 nm particles only. In time course experiments, both these peaks appear in the spectra collected at 5 min and grow in over time (See Figure 3.13 and 3.14). Therefore, these are assigned to citric acid adsorbed on specific binding sites available on these very small ceria nanoparticles.[24] Furthermore, the appearance of similar differences for the smallest nanoceria investigated upon adsorption of acetic acid provides additional

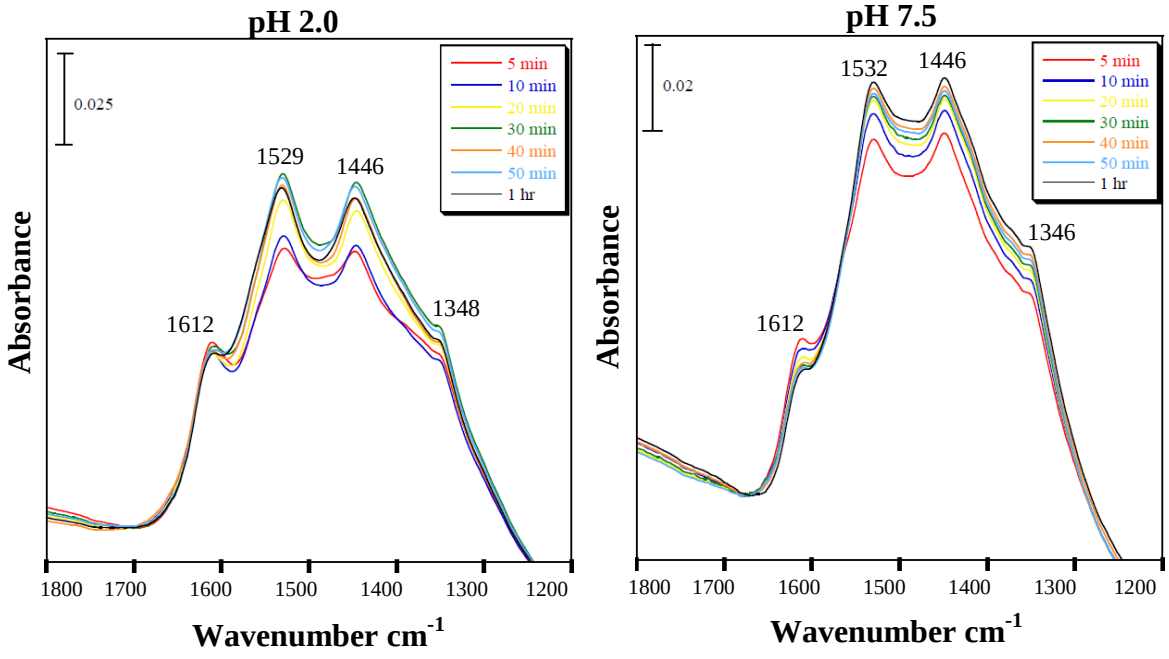

Figure 3.15. ATR-FTIR spectra of adsorbed acetic acid on 4 nm CeO_2 at pH 2.0 and 7.5

evidence that these new absorption bands are due to adsorbed carboxylate groups (Figure 3.15). The acetic acid solution spectra are given in Figure 3.16 and the peak assignments are listed in Table 3.2. These are potentially corner and edge sites that are more prevalant on very small nanoparticles and it may be these sites that become important in adsorption on 4 nm particles.[45]

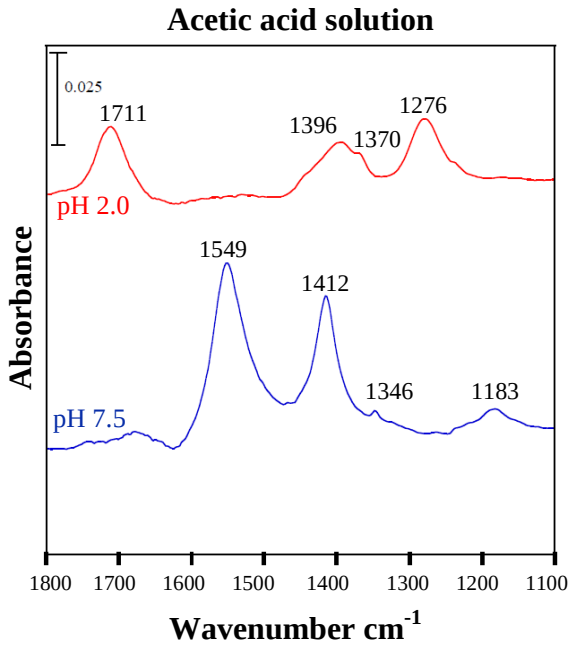

Figure 3.16. ATR-FTIR spectra of acetic acid solution (100 mM) at pH 2.0 and 7.5

In determining the adsorption mode of carboxylate acids on metal oxide surfaces, the Δν value, [$\nu_{as}COO^-$ - ν_sCOO^-], has been used as a probe and measure of the interaction of adsorbed carboxylate groups.[25-29, 31] In the spectra shown for the 9 nm sample at all pHs as well as the spectrum of 4 nm sample at pH 7.5, a Δν value of ~170 cm^{-1} is found which suggests bidentate bridging adsorption of the carboxylate groups. For

Table 3.3. Vibrational frequencies (cm^{-1}) and assignment of the solution phase acetic acid

Wavenumber (cm^{-1})	**Assignment**
1711	-C=O stretching
1549	$-COO^-$ Asymmetric stretching
1396, 1412	$-COO^-$ symmetric stretching
1370	$-CH_3$ stretching
1346	$-CH_2-$ rocking
1276	-C-O stretching
1183	-C-C- stretching

the spectra obtained for the smaller 4 nm sample at the other three pHs investigated, two$\Delta\nu$ values are identified, one with the $\Delta\nu$ value of ~170 cm^{-1}, similar to what is noted above for bridging adsorption, and another with much larger $\Delta\nu$ value of 245 cm^{-1}. This suggests that in addition to the bridging carboxylate groups, singly bonded carboxylate groups exist on these very small ceria nanoparticles and as noted above, most likely occurring on the corner and edge sites at the higher coverages found for these lower pHs (*vide infra*). A summary of variation of citric acid over pH 2.0 to 7.5 is given in Figure 3.17.

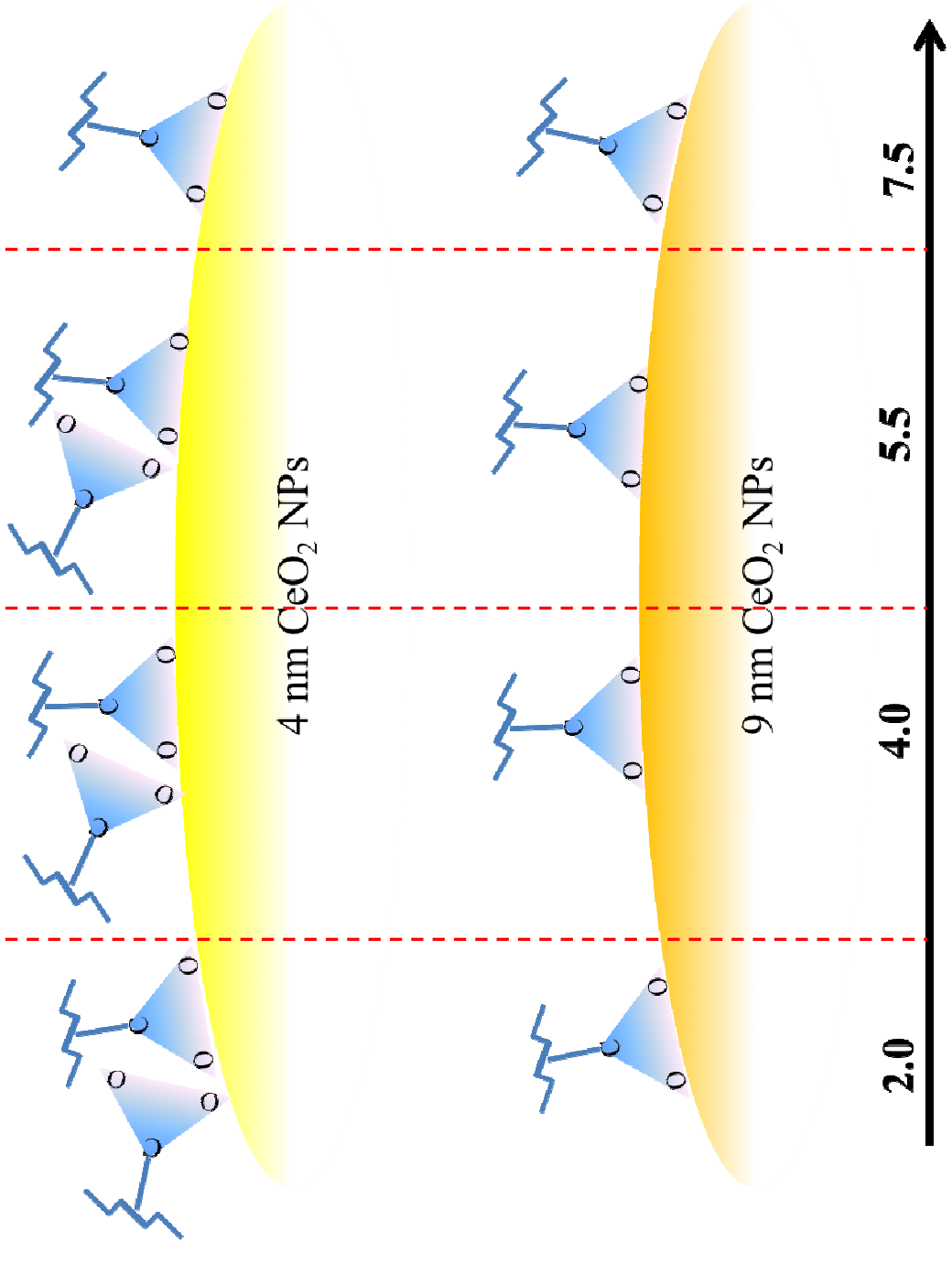

Figure 3.17. Summary of binding modes of citric acid on 4 nm and 9 nm CeO_2 at different pHs: 2.0, 4.0, 5.5 and 7.5

3.4 Citric Acid Adsorption on CeO_2 Nanoparticles: Measurements of Surface Coverage as a *f*(pH)

Citric acid adsorption on 4, 9 and 39 nm CeO_2 nanoparticles was carried out at pH 2.0, 4.0, 5.5 and 7.5 (and it should be noted that pH remained constant in these experiments). The mass and the surface area normalized uptake of citric acid at saturation coverage are given in Table 3.3. Saturation coverage was determined to occur at concentrations greater than 8 mM and these values represent the average of three different independent measurements of solution phase concentration at 10 mM citric acid. The decrease in mass normalized and surface area normalized surface coverage with increasing pH is expected, because the surface charge of both ceria and citric acid species increases with increasing pH thereby increasing the repulsion between them. However, they are also higher for the 9 nm particles compared to that of 4 nm particles. This can be either due to the fact that the aggregation of nanoparticles is higher in smaller nanoparticles or due to some special binding sites available on these 9 nm ceria particles. Further, the special edge and corner sites on these nanoparticles can contribute for more reactive sites as explained by Klabunde and the co-workers.[46] In addition, on these 9 nm CeO_2 particles on which the citric acid binds only in the bridging mode, the adsorbed citric acid species form more uniform layers thereby allowing multiple layer adsorptions to occur. However, as citric acid species bind on 4 nm CeO_2 nanoparticles in both bridging and singly bound modes the adsorbate layers are irregular thereby restricting the multiple layer formation. This may be another reason for observing higher adsorption on 9 nm particles compared to 4 nm particles. However, the effective surface areas of these

nanoparticles in solution are unknown. Even the 39 nm samples, which did not show any adsorption in ATR-FTIR spectra, also show some uptake of citric acid.

Table 3.4. Quantitative measurements of surface saturation coverages for citric acid adsorption on nanoceria as a function of pH and particle size

pH	Surface saturation coverage					
	4 nm		9 nm		39 nm	
	mmol/g	molecules/cm^2 ($\times 10^{14}$)	mmol/g	molecules/cm^2 ($\times 10^{14}$)	mmol/g	molecules/cm^2 ($\times 10^{14}$)
2.0	0.49 ± 0.02	3.7 ± 0.3	0.61 ± 0.05	5.9 ± 0.9	0.48 ± 0.04	51.9 ± 4.5
4.0	0.39 ± 0.02	2.9 ± 0.3	0.38 ± 0.02	3.7 ± 0.5	0.17 ± 0.05	18.5 ± 5.6
5.5	0.29 ± 0.14	2.2 ± 1.0	0.28 ± 0.08	2.7 ± 0.8	0.16 ± 0.06	17.2 ± 6.1
7.5	0.12 ± 0.07	0.92 ± 0.6	-	-	-	-

3.5 Nanoparticle-Nanoparticle Interactions, Nanoparticle Aggregation and Colloidal Stability

Sedimentation studies and zeta potential measurements were carried out at the same conditions at which the quantitative adsorption measurements were taken.

Sedimentation patterns as a function of time for the three CeO_2 nanoparticle types, both in the presence and the absence of citric acid, are shown in Figure 3.10. In these experiments, stable suspensions will have stable light scattering resulting in an A/A_o values that are constant whereas unstable suspensions that form aggregates that settle out will show a decrease in A/A_o.

Sedimenation plots, i.e. A/A_o as a function of time, show that in the absence of citric acid, 4 nm and 9 nm CeO_2 nanoparticles of 1.0 g/L concentration settle out from the solutions at pH 4.0, 5.5 and 7.5, whereas both of them form stable suspensions at pH 2.0. At pH 2.0, the protonated CeO_2 particles experience higher repulsive forces and hence an increase in the double layer formation which will allow it to form stable suspensions.[23] However, at higher pHs the surface charge shifts towards neutral and the double layer decreases. Thus the aggregation of nanoparticles at pH 4.0, 5.5 and 7.5 is higher, resulting in the sedimentation patterns reported here. It is found that the larger 39 nm ceria particles settled out under all conditions. . This can be because of the gravitational settling down of these nanoparticles irrespective of the solution conditions applied.

Most interesting is the fact that these sedimentation patterns completely reverse for all three sizes of nanoceria in the presence of citric acid, as shown in Figure 3.10. Based on the speciation of citric acid on ceria surface as evidenced by spectroscopic data, this reversal can be attributed to the change in the surface charge in the presence of citric acid.[23] In fact zeta potential measurements support this argument. In general, zeta potential measures the net charge at the diffuse boundary of a particle. The general trend is that the particles with zeta potential closer to zero form unstable suspensions. Figure 3.11 shows the differences in the zeta potential for CeO_2 particles measured in the

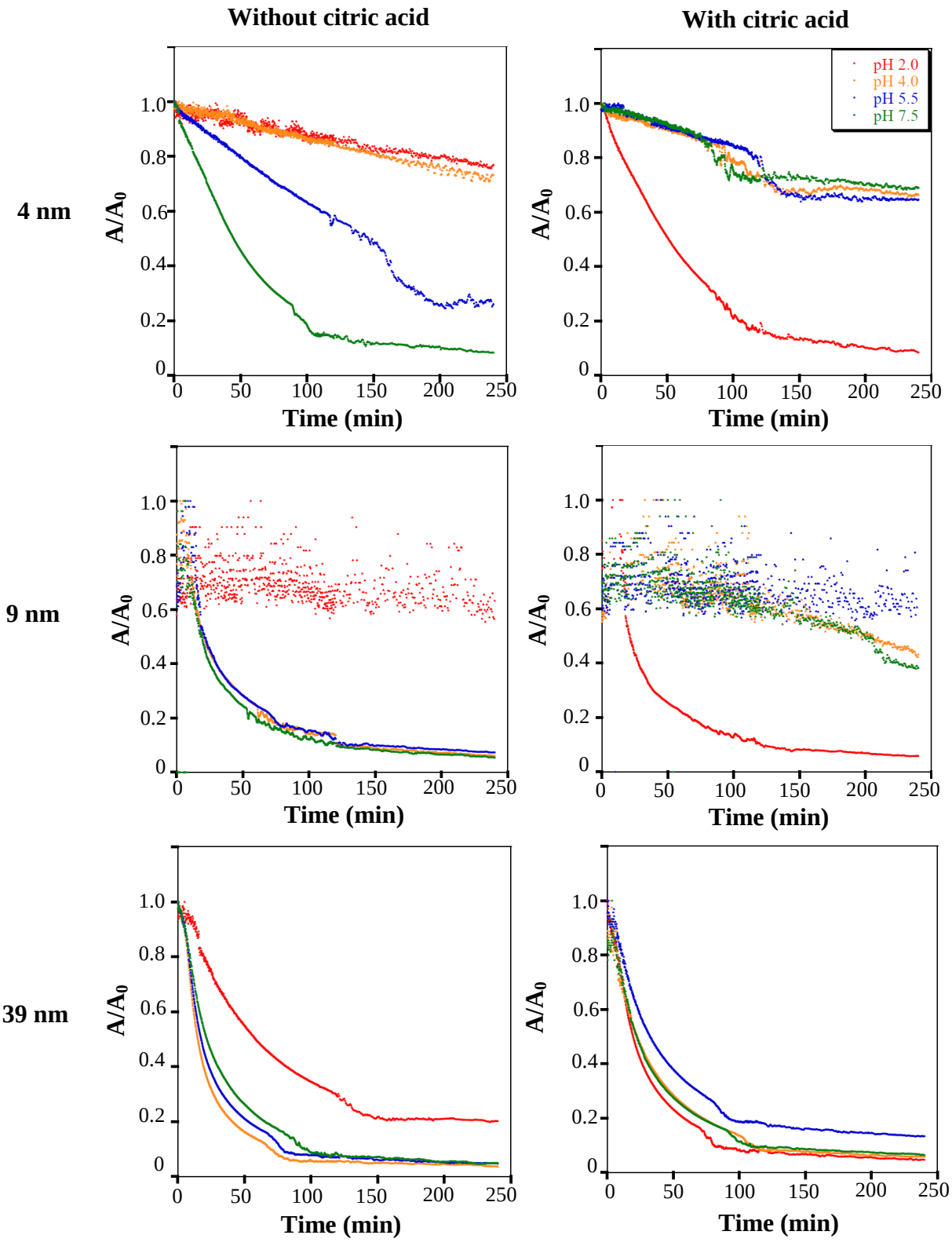

Figure 3.18. Sedimentation of 4, 9 and 39 nm CeO_2 in the absence and the presence of citric acid at pH 2.0 (red), 4.0 (orange), 5.5 (blue) and 7.5 (green).

presence and the absence of citric acid. These results show that after citric acid adsorption the measured zeta potentials decrease at all four pH values and have absolute

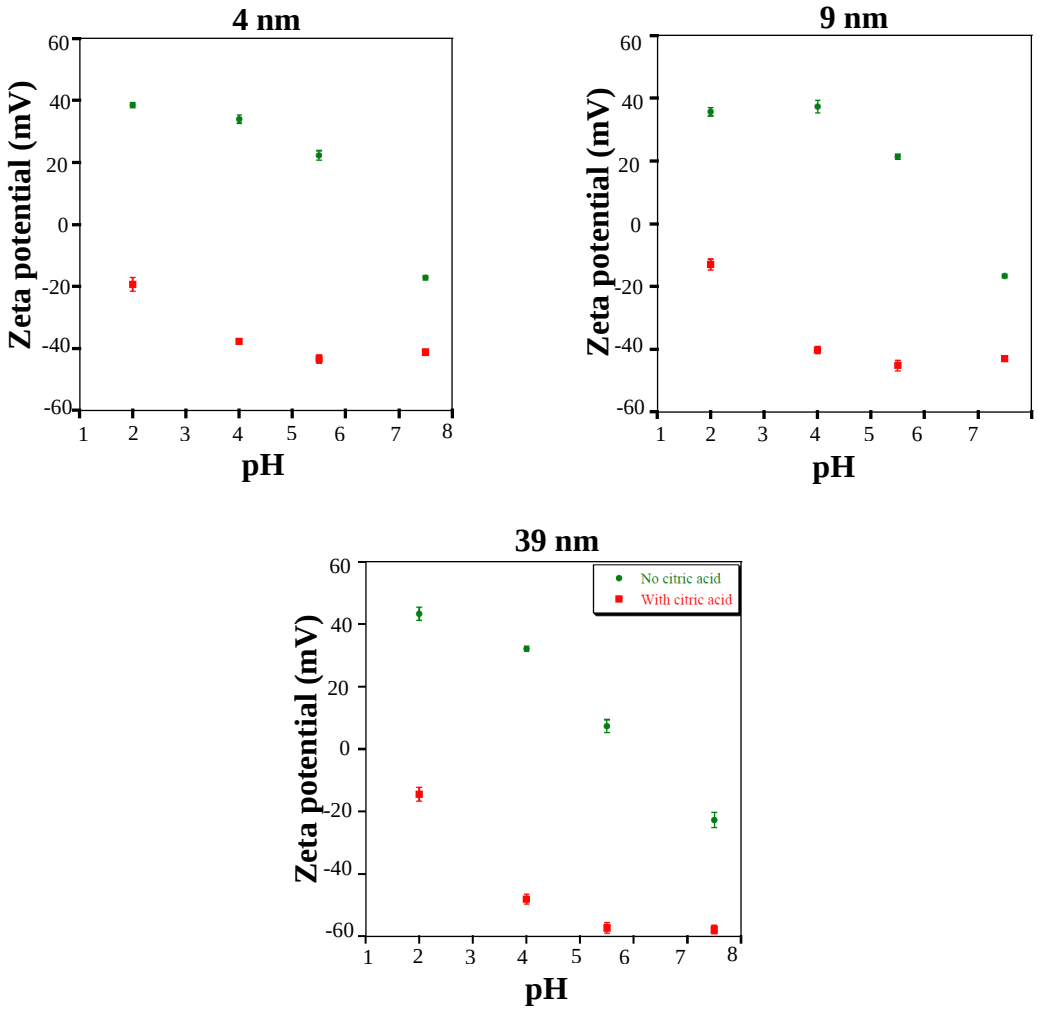

Figure 3.19. Zeta potential measurements of CeO_2 (1.0 g/L) in the absence (green) and the presence (red) of citric acid (1.0 mM) as a function of pH.

values closer to zero. At pH 2.0 zeta potential changes from +38 to -19, +36 to -13 and 43 to -14 for 4, 9 and 39 nm CeO_2 respectively, thereby decreasing the suspension stability as evidenced by sedimentation plots. However, upon citric acid adsorption at pH 7.5 shifts the zeta potential to more negative values from -17 to -41, -17 to -43 and -23 to -58 for 4, 9 and 39 nm CeO_2 respectively and thus the absolute magnitude of the zeta potential is much larger and these colloidal suspensions become more stable due to the larger repulsive electrostatic interactions between nanoparticles. These results follow a very similar trend found for 4 nm TiO_2 nanoparticles upon adsorption of citric acid.[23]

3.6. Quantification of adsorption by X-ray Photoelectron Spectroscopy

The adsorption of citric acid on nanoceria surface was quantified as an increased percentage of surface area under the peak at 289 eV in C 1s XPS spectra compared to that of initial C 1s XPS spectra at pH 2.0 and 7.5. The obtained values are summarized in the Table 3.4.

Table 3.5. Increase in surface area under the peak 289 eV of C 1s XPS spectra due to citric acid adsorption

CeO_2 Sample	**Increase in C/Ce ratio after citric acid adsorption (%)**	
	pH 2.0	**pH 7.5**
4 nm	61 ± 0.3	21 ± 0.3
9 nm	43 ± 0.2	17 ± 0.3
39 nm	36 ± 0.2	13 ± 0.2

The data show that the amount of adsorption correlates with the particle size; higher the particle size lower the adsorption and vice versa. However, these results contradict the quantification data from the HPLC measurements. This may be due to the fact that, as the citric acid adsorbed CeO_2 samples are washed before XPS analysis, the physisorbed multiple layers on 9 nm ceria are washed out accounting only for the monolayer of adsorbates on the nanoparticle thereby contributing for a lower amount of adsorbates.

CHAPTER 4

CONCLUSIONS AND ENVIRONMENTAL IMPLICATIONS

This study brings out several conclusions about the surface adsorption and surface chemistry of citric acid on nanoceria as a function of size and pH as well as its impact on nanoparticle-nanoparticle interactions and colloidal solution stability. First, even though citric acid solution speciation is highly pH dependent in the range investigated here (2.0-7.5), fully deprotonated form of citric acid was prominent as the adsorbed species at all pHs investigated. Second, the binding mode was different for the smallest nanparticle, 4 nm, having both bridging and singly bound carboxylates whereas 9 nm particles showed only the presence of bridged carboxylates. Third, surface coverage was pH dependent with a maximum coverage at the lowest pH. Fourth, the aggregation of ceria nanoparticles is a function of pH, which is highest around pH_{zpc}. However, the presence of adsorbed citrate changes the aggregation behavior by altering the surface charge of the nanoparticle. As a result, suspensions that are relatively stable at pH 2.0 in the absence of citric acid are destabilized forming aggregates that undergo flocculation and settle out over time. In contrast, pH 7.5 aggregates form in the absence of citric acid yet upon citrate adsorption stable suspensions. Thus surface adsorption, surface charge and pH have an important and direct impact on the behavior of nanoceria and its distribution in the aquatic environments including cellular matrices. Figure 4.1 provide a brief summary of these results.

In addition, a comment on Aldrich CeO_2 nanoparticle sample should be made at this point. Being a highly polydispersed sample, the quantification of citric acid adsorption on these nanoparticles remains inconclusive. And also showing no ATR-FTIR

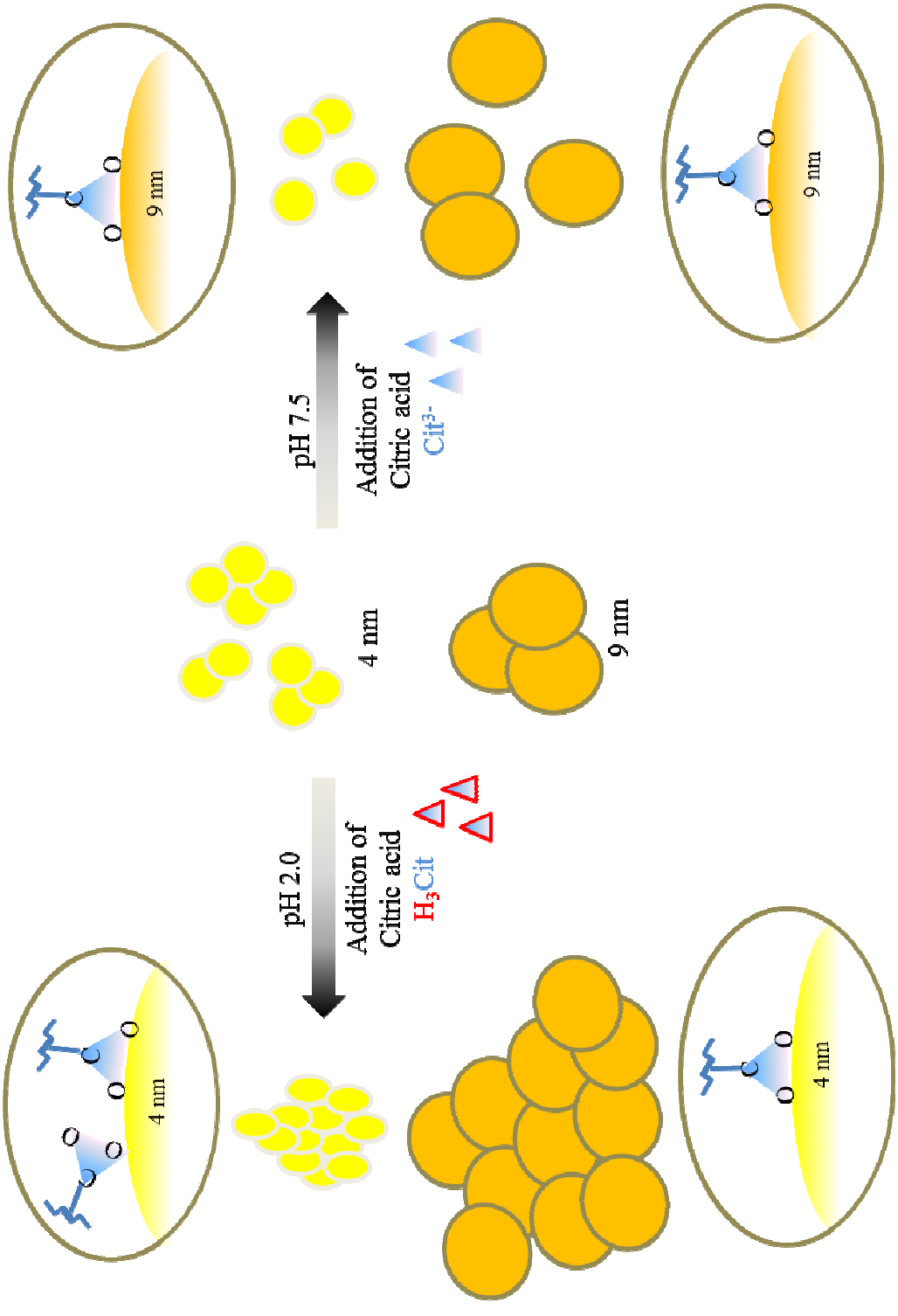

Figure 4.1. Summary of the behavior of nanoceria in the presence of citric acid at acidic and circumneutral pH

spectrum, gravitational settling down of the particle irrespective of the conditions applied and showing an organic impurity in the C 1s XPS spectrum makes the interpretation of the behavior of these nanoparticles in the studied solution systems complex.

The trends observed in the aggregation pattern of nanoceria in the presence and the absence of citric acid are of environmental and biological significance as aggregation play a key role in the distribution of these particles in aquatic environments as well as in biological matrices (Figure 4.2). Additionally, these studies provide important information on the potential use of citric acid as a coating material for nanoceria in biomedical applications.

Furthermore, it is well known that the nanomaterials are being increasingly used for wide variety of applications. Nanoceria currently play a key role in catalysts, fuel cells, optical polishing and semiconductor industries. With this increasing use the studies to understand the behavior of these engineered NPs in the environment are of high demand. However, the understanding of the behavior of them, especially in natural water systems, is complex due to a number of factors including pH, ionic strength and the presence of complexing ligands.[23] In addition nanoparticle aggregation adds to the complexity and questions the validity of high concentration-toxicity relationships due to a potential decrease in bioavailability of the aggregated particles. Therefore the studies like this, in which the behavior of nanoparticles in simpler aquatic systems are monitored, become important and provide valuable insights into their behavior in complex matrices found in nature.

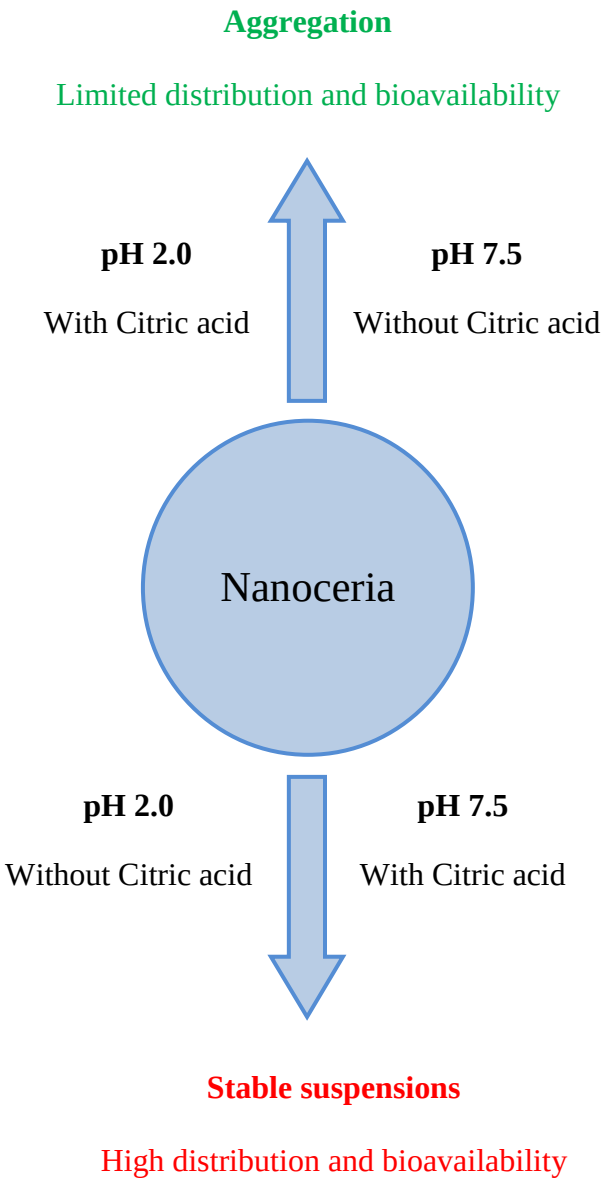

Figure 4.2. Aggregation pattern of nanoceria in the presence and the absence of citric acid as a function of pH

REFERENCES

1. Cao, G., *Nanostructures & nanomaterials : synthesis, properties & applications*. Imperial College Press: London, 2007.

2. Nowack, B.; Bucheli, T. D., Occurrence, behavior and effects of nanoparticles in the environment. *Environmental Pollution* **2007,** 150, (1), 5-22.

3. Mudunkotuwa, I. A.; Grassian, V. H., The devil is in the details (or the surface): impact of surface structure and surface energetics on understanding the behavior of nanomaterials in the environment. *Journal of Environmental Monitoring* **2011,** 13, (5), 1135-1144.

4. Grassian V. H., Size-Dependent Properties and Surface Chemistry of Oxide-Based Nanomaterials in Environmental Processes. In *Nanoscale Materials in Chemistry: Environmental Applications,* American Chemical Society: 2010; Vol. 1045, pp 15-33.

5. Kaegi, R.; Ulrich, A.; Sinnet, B.; Vonbank, R.; Wichser, A.; Zuleeg, S.; Simmler, H.; Brunner, S.; Vonmont, H.; Burkhardt, M.; Boller, M., Synthetic TiO_2 nanoparticle emission from exterior facades into the aquatic environment. *Environmental Pollution* **2008,** 156, (2), 233-239.

6. Zheng, N.; Wang, H. J., Discovery of Anatase in Atmospheric Inhalable Particles and Its Significance. *Spectroscopy and Spectral Analysis* **2009,** 29, (6), 1570-1572.

7. Klaine, S. J.; Alvarez, P. J. J.; Batley, G. E.; Fernandes, T. F.; Handy, R. D.; Lyon, D. Y.; Mahendra, S.; McLaughlin, M. J.; Lead, J. R., Nanomaterials in the environment: Behavior, fate, bioavailability, and effects. *Environmental Toxicology and Chemistry* **2008,** 27, (9), 1825-1851.

8. Biskos, G.; Schmidt-Ott, A., Airborne Engineered Nanoparticles: Potential Risks and Monitoring Challenges for Assessing their Impacts on Children. *Paediatric Respiratory Reviews* **2012,** 13, (2), 79-83.

9. Colvin, V. L., The potential environmental impact of engineered nanomaterials. *Nat Biotech* **2003,** 21, (10), 1166-1170.

10. Grassian, V. H., When Size Really Matters: Size-Dependent Properties and Surface Chemistry of Metal and Metal Oxide Nanoparticles in Gas and Liquid Phase Environments. *The Journal of Physical Chemistry C* **2008,** 112, (47), 18303-18313.

11. Rodriguez; J. A.; Xianqin, W.; Hanson; Jonathan, C.; Gang, L. I. U.; Iglesias, J.; Ana; Fernandez, G.; Marcos, The behavior of mixed-metal oxides: Structural and electronic properties of $Ce_{1-x}Ca_xO_2$ and $Ce_{1-x}Ca_xO_{2-x}$. **2003,** 119, 11.

12. Sameer, D.; Swanand, P.; Satyanarayana, V. N. T. K.; Sudipta, S., Size dependency variation in lattice parameter and valency states in nanocrystalline cerium oxide. *Applied Physics Letters* **2005,** 87, (13), 133113.

13. Hoecke, K. V.; Quik, J. T. K.; Mankiewicz-Boczek, J.; Schamphelaere, K. A. C. D.; Elsaesser, A.; Meeren, P. V. d.; Barnes, C.; McKerr, G.; Howard, C. V.; Meent, D. V. D.; RydzynÌ ski, K.; Dawson, K. A.; Salvati, A.; Lesniak, A.; Lynch, I.; Silversmit, G.; Samber, B. r. D.; Vincze, L.; Janssen, C. R., Fate and Effects of CeO_2 Nanoparticles in Aquatic Ecotoxicity Tests. *Environmental Science & Technology* **2009,** 43, (12), 4537-4546.

14. Zhang, F.; Jin, Q.; Chan, S.-W., Ceria nanoparticles: Size, size distribution, and shape. *Journal of Applied Physics* **2004,** 95, (8), 4319-4326.

15. Spanier, J. E.; Robinson, R. D.; Zhang, F.; Chan, S.-W.; Herman, I. P., Size-dependent properties of CeO_{2-y} nanoparticles as studied by Raman scattering. *Physical Review B* **2001,** 64, (24), 245407.

16. Ivanov, V. K; Shcherbakov, A. B.; Usatenko, A. V. Structure-sensitive properties and biomedical applications of nanodispersed cerium dioxide. *Russian Chemical Reviews* **2009,** 78, (9), 855.

17. Cornelis, G.; Ryan, B.; McLaughlin, M. J.; Kirby, J. K.; Beak, D.; Chittleborough, D., Solubility and Batch Retention of CeO_2 Nanoparticles in Soils. *Environmental Science & Technology* **2011,** 45, (7), 2777-2782.

18. Zhang, H.; He, X.; Zhang, Z.; Zhang, P.; Li, Y.; Ma, Y.; Kuang, Y.; Zhao, Y.; Chai, Z., Nano-CeO_2 Exhibits Adverse Effects at Environmental Relevant Concentrations. *Environmental Science & Technology* **2011,** 45, (8), 3725-3730.

19. Xia, T.; Kovochich, M.; Liong, M.; MaÌˆdler, L.; Gilbert, B.; Shi, H.; Yeh, J. I.; Zink, J. I.; Nel, A. E., Comparison of the Mechanism of Toxicity of Zinc Oxide and Cerium Oxide Nanoparticles Based on Dissolution and Oxidative Stress Properties. *ACS Nano* **2008,** 2, (10), 2121-2134.

20. Patil, S.; Sandberg, A.; Heckert, E.; Self, W.; Seal, S., Protein adsorption and cellular uptake of cerium oxide nanoparticles as a function of zeta potential. *Biomaterials* **2007,** 28, (31), 4600-4607.

21. Horie, M.; Nishio, K.; Fujita, K.; Endoh, S.; Miyauchi, A.; Saito, Y.; Iwahashi, H.; Yamamoto, K.; Murayama, H.; Nakano, H.; Nanashima, N.; Niki, E.; Yoshida, Y., Protein Adsorption of Ultrafine Metal Oxide and Its Influence on Cytotoxicity toward Cultured Cells. *Chemical Research in Toxicology* **2009,** 22, (3), 543-553.

22. Limbach, L. K.; Li, Y.; Grass, R. N.; Brunner, T. J.; Hintermann, M. A.; Muller, M.; Gunther, D.; Stark, W. J., Oxide Nanoparticle Uptake in Human Lung Fibroblasts: Effects of Particle Size, Agglomeration, and Diffusion at Low Concentrations. *Environmental Science & Technology* **2005,** 39, (23), 9370-9376.

23. Mudunkotuwa, I. A.; Grassian, V. H., Citric Acid Adsorption on TiO_2 Nanoparticles in Aqueous Suspensions at Acidic and Circumneutral pH: Surface Coverage, Surface Speciation, and Its Impact on Nanoparticle-Nanoparticle Interactions. *Journal of the American Chemical Society* **2010,** 132, (42), 14986-14994.

24. Pettibone, J. M.; Cwiertny, D. M.; Scherer, M.; Grassian, V. H., Adsorption of Organic Acids on TiO_2 Nanoparticles: Effects of pH, Nanoparticle Size, and Nanoparticle Aggregation. *Langmuir* **2008,** 24, (13), 6659-6667.

25. Ojamae, L.; Aulin, C.; Pedersen, H.; Kall, P-O., IR and quantum-chemical studies of carboxylic acid and glycine adsorption on rutile TiO_2 nanoparticles. *Journal of Colloid and Interface Science* **2006,** 296, (1), 71-78.

26. Brownson, J. R. S.; Tejedor-Tejedor, M. I.; Anderson, M. A., FTIR Spectroscopy of Alcohol and Formate Interactions with Mesoporous TiO_2 Surfaces. *The Journal of Physical Chemistry B* **2006,** 110, (25), 12494-12499.

27. Guan, X.-h.; Chen, G.-h.; Shang, C., ATR-FTIR and XPS study on the structure of complexes formed upon the adsorption of simple organic acids on aluminum hydroxide. *Journal of Environmental Sciences* **2007,** 19, (4), 438-443.

28. Duckworth, O. W.; Martin, S. T., Surface complexation and dissolution of hematite by C_1-C_6 dicarboxylic acids at pH = 5.0. *Geochimica et Cosmochimica Acta* **2001,** 65, (23), 4289-4301.

29. Hwang, Y. S.; Liu, J.; Lenhart, J. J.; Hadad, C. M., Surface complexes of phthalic acid at the hematite/water interface. *Journal of Colloid and Interface Science* **2007,** 307, (1), 124-134.

30. Hwang, Y. S.; Lenhart, J. J., Adsorption of C4-Dicarboxylic Acids at the Hematite/Water Interface. *Langmuir* **2008,** 24, (24), 13934-13943.

31. Dobson, K. D.; McQuillan, A. J., In situ infrared spectroscopic analysis of the adsorption of aliphatic carboxylic acids to TiO_2, ZrO_2, Al_2O_3, and Ta_2O_5 from aqueous solutions. *Spectrochimica Acta Part A: Molecular and Biomolecular Spectroscopy* **1999,** 55, 1395-1405.

32. Sehgal, A.; Lalatonne, Y.; Berret, J. F.; Morvan, M., Precipitationâ^'Redispersion of Cerium Oxide Nanoparticles with Poly(acrylic acid): Toward Stable Dispersions. *Langmuir* **2005,** 21, (20), 9359-9364.

33. Fresnais, J.; Lavelle, C.; Berret, J. F., Nanoparticle Aggregation Controlled by Desalting Kinetics. *The Journal of Physical Chemistry C* **2009,** 113, (37), 16371-16379.

34. Safi, M.; Sarrouj, H.; Sandre, O.; Mignet, N.; Berret, J-F., Interactions between sub-10-nm iron and cerium oxide nanoparticles and 3T3 fibroblasts: the role of the coating and aggregation state. *Nanotechnology* **2010,** 21, (14), 145103.

35. Masui, T.; Hirai, H.; Imanaka, N.; Adachi, G.; Sakata, T.; Mori, H., Synthesis of cerium oxide nanoparticles by hydrothermal crystallization with citric acid. *Journal of Materials Science Letters* **2002,** 21, (6), 489-491.

36. Ma, J.; Qian, K.; Huang, W.; Zhu, Y.; Yang, Q., Facile One-Step Synthesis of Double-Shelled CeO_2 Hollow Spheres and Their Optical and Catalytic Properties. *Bulletin of the Chemical Society of Japan* **2010,** 83, (12), 1455-1461.

37. Li, S.; Zheng, J.; Yang, W.; Zhao, Y.; Liu, Y., Preparation and characterization of three-dimensional ordered macroporous rare earth oxide—CeO_2. *Journal of Porous Materials* **2008,** 15, (5), 589-592.

38. Naik, Y.; Ramarao, G.; Banthiya, A.; Chaudhary, D.; Arora, C., Synthesis and characterization of nano-structured $Th_{1-x}Ce_xO_2$; mixed oxide. *Journal of Thermal Analysis and Calorimetry* **2012,** 107, (1), 105-110.

39. Baltrusaitis, J.; Cwiertny, D. M.; Grassian, V. H., Adsorption of sulfur dioxide on hematite and goethite particle surfaces. *Physical Chemistry Chemical Physics* **2007,** 9, (41), 5542-5554.

40. Baltrusaitis, J.; Jayaweera, P. M.; Grassian, V. H., Sulfur Dioxide Adsorption on TiO_2 Nanoparticles: Influence of Particle Size, Coadsorbates, Sample Pretreatment, and Light on Surface Speciation and Surface Coverage. *The Journal of Physical Chemistry C* **2011,** 115, (2), 492-500.

41. Dutta, P.; Pal, S.; Seehra, M. S.; Shi, Y.; Eyring, E. M.; Ernst, R. D., Concentration of Ce^{3+} and Oxygen Vacancies in Cerium Oxide Nanoparticles. *Chemistry of Materials* **2006,** 18, (21), 5144-5146.

42. Burroughs, P.; Hamnett, A.; Orchard, A. F.; Thornton, G., Satellite structure in the X-ray photoelectron spectra of some binary and mixed oxides of lanthanum and cerium. *Journal of the Chemical Society, Dalton Transactions* **1976**, (17), 1686-1698.

43. Zhang, F.; Wang, P.; Koberstein, J.; Khalid, S.; Chan, S.-W., Cerium oxidation state in ceria nanoparticles studied with X-ray photoelectron spectroscopy and absorption near edge spectroscopy. *Surface Science* **2004,** 563, 74-82.

44. Pasilis, S. P.; Pemberton, J. E., Spectroscopic investigation of uranyl(VI) and citrate coadsorption to Al2O3. *Geochimica et Cosmochimica Acta* **2008,** 72, (2), 277-287.

45. Erickson, L. E.; Koodali, R. T.; Richards, R.; American Chemical Society. Division of Industrial and Engineering, C., *Nanoscale materials in chemistry : environmental applications*. American Chemical Society ; Distributed by Oxford University Press: Washington, DC; [New York], 2010.

46. Stark, J. V.; Park, D. G.; Lagadic, I.; Klabunde, K. J., Nanoscale Metal Oxide Particles/Clusters as Chemical Reagents. Unique Surface Chemistry on Magnesium Oxide As Shown by Enhanced Adsorption of Acid Gases (Sulfur Dioxide and Carbon Dioxide) and Pressure Dependence. *Chemistry of Materials* **1996,** 8, (8), 1904-1912.